TECHNICAL REPORT

MULTISCALE AIR QUALITY SIMULATION PLATFORM

(MAQSIP):

SOURCE CODE DOCUMENTATION AND VALIDATION

M. Talat Odman
Clint L. Ingram
Environmental Programs
MCNC–North Carolina Supercomputing Center
P.O. Box 12889
Research Triangle Park, NC 27709-2889

ABSTRACT

Multiscale **A**ir **Q**uality **SI**mulation **P**latform (MAQSIP) is a generalized coordinate chemistry transport model following the transformed equations of Srivastava et al (1994). MAQSIP solves the atmospheric diffusion equation in a user-specified coordinate system using process splitting. This generalization allows MAQSIP to be applied to almost any practical coordinate systems. Currently, the hydrostatic (RADM-type) and non-hydrostatic (SAQM-type) sigma-pressure coordinate systems have been applied. However, MAQSIP can be formulated with other coordinate systems by simply providing the coordinate dependent modules.

ACKNOWLEDGMENTS

MAQSIP: SOURCE CODE DOCUMENTATION AND VALIDATION

CONTENTS

Section 1: Introduction

MAQSIP is a state-of-the-art pollutant transport/chemistry modeling platform. The following attributes of MAQSIP distinguish it from its current counterparts.

1) **Modular**: MAQSIP is a truly modular platform where physical/chemical processes are cast into modules following the time-splitting approach. Each process module operates on a common concentration field. Other variables are encapsulated within each module.

2) **Flexible**: MAQSIP has alternative modules for various processes.

3) **Expandable**: New modules can be (and are being) added to the platform by scientists using MAQSIP in their research.

4) **Multiscale**: MAQSIP supports multiple, multi-level nested grids.

5) **Generalized Coordinates**: MAQSIP can support practically any coordinate system.

This document describes the basic modules of MAQSIP with emphasis on the generalized coordinate feature. This feature (and the presence of alternative modules) allows MAQSIP to unify various existing models within the same platform. Using the modules described within this report, both the Regional Acid Deposition Model (RADM) and the SARMAP Air Quality Model (SAQM) have been emulated and very similar performance is observed in application.

In Section 2, the generalized coordinate formulation is summarized. The reader is referred to Srivastava et al. (1994) for the details of the derivation and a complete list of assumptions. Section 3 reviews the two coordinate systems currently implemented in Version 2.1 of MAQSIP. Again, Srivastava et al. should be consulted for other coordinate system possibilities. Sections 4 and 5 describe the modules of MAQSIP by categorizing them as coordinate independent and coordinate dependent. The necessary parameters and input data are described in Sections 6 and 7, respectively. Section 8 contains model evaluation and validation information. Finally, summary information is given in condensed tabular form in the appendices.

SECTION 2: ATMOSPHERIC DIFFUSION EQUATION

As derived in Srivastava et al (1994), the species continuity equation (flux-form) in generalized coordinates can be written as:

$$\frac{\partial}{\partial t}\left(\sqrt{\gamma}\,\overline{c_i}\right)+\frac{\partial}{\partial x^j}\left(\sqrt{\gamma}\,\overline{c_i}\,\overline{v^j}\right)+\frac{\partial}{\partial x^j}\left(\sqrt{\gamma}\,\overline{c_i'\,v^{j'}}\right)=\sqrt{\gamma}\,R_i+\sqrt{\gamma}\,S_i,\,(j=1,2,3) \qquad (2.1)$$

where,

γ is the determinant of the metric tensor

c_i is the concentration (mass volume) of pollutant i

x^j is the jth coordinate ($j=1,2,3$)

v^j is the contravariant velocity (i.e., the component of the velocity vector in x^j-direction)

R_i is the chemical formation or loss rate of pollutant i

S_i is the source/sink term for pollutant i

$\overline{}$ denotes mean

'   denotes fluctuation about mean

Furthermore, turbulent diffusion is parameterized as:

$$\overline{c_i'\,v^{j'}} \approx \overline{\rho}\left[-K^{ij}\frac{\partial}{\partial x^j}\left(\frac{\overline{c_i}}{\overline{\rho}}\right)\right] \qquad (2.2)$$

K^{ij} is the contravariant diffusivity (i.e., components of diffusivity tensor in the $x^j \cdot x^j$-direction)

ρ is the density of air/pollutant mixture

MAQSIP solves the following equation, which is obtained by substituting Equation (2.2) into Equation (2.1).

3

$$\frac{\partial}{\partial t}\left(\sqrt{\gamma}\ \overline{c_i}\right)+\frac{\partial}{\partial x^j}\left(\sqrt{\gamma}\ \overline{c_i}\ \overline{v^j}\right)+\frac{\partial}{\partial x^j}\left[-\sqrt{\gamma}\ \overline{\rho}\ K^{jj}\frac{\partial}{\partial x^j}\left(\frac{\overline{c_i}}{\overline{\rho}}\right)\right]=\sqrt{\gamma}\,R_i+\sqrt{\gamma}\,S_i \qquad (2.3)$$

SECTION 3: COORDINATE SYSTEMS

MAQSIP (Version 2.1) can currently be configured with conformal mapped coordinates in the horizontal (e.g., Lambert Conformal, Polar Stereographic, and Mercator) and two different coordinate systems in the vertical: the hydrostatic and non-hydrostatic sigma-pressure coordinate systems. The hydrostatic sigma-pressure coordinates is also used in the Regional Acid Deposition Model (RADM) (Chang et al., 1987). The non-hydrostatic sigma-pressure coordinate system is the coordinate system used in the SARMAP Air Quality Model (SAQM) (Jin and Chang, 1993). Both of these coordinate systems are described in this section and cast into the generalized coordinates form $\left(x^1, x^2, x^3\right)$ of MAQSIP. The terms γ and v^j denote the determinant of the metric tensor and the contravariant velocity, respectively, for a given coordinate system. The expressions for each of these terms will be given below for each of the two coordinate systems currently supported by MAQSIP. These expressions can then be substituted in Equation (2.1) to derive the atmospheric diffusion equation in the coordinate system of interest. Further, if K-theory (i.e., Equation 2.2) is used for parameterizing turbulent diffusion, Equation (2.3) can be used. The contravariant diffusivities, K^{ij}, are also given below for the two coordinate systems. A full derivation of the relevant terms for these coordinate systems and the parameterization of the turbulent diffusion can be found in Srivastava et al (1994).

3.1 HYDROSTATIC SIGMA-PRESSURE COORDINATES

MAQSIP can be configured to utilize the conformal mapped coordinates (Lambert Conformal) in the horizontal with a sigma-pressure coordinate in the vertical. MAQSIP defines this coordinate system as:

$$x^1 = x_m$$
$$x^2 = y_m \qquad\qquad (3.1.1)$$
$$x^3 = 1 - \sigma \,;\ \ \sigma = \frac{p - p_T}{p^*}$$

where $\left(x_m, y_m, z_m\right)$ denote the conformal mapped coordinate system, $p(x_m, y_m, z_m, t)$ is the pressure, p_T is the pressure at the model top and is held constant, $p^* = p_S - p_T$, and $p_S(x_m, y_m, t)$ is the surface pressure.

MAQSIP assumes that the atmosphere is hydrostatic. Under this assumption, the vertical momentum equation reduces to:

$$\frac{\partial p}{\partial z_m} = -\rho g \tag{3.1.2}$$

Therefore,

$$\frac{\partial x^3}{\partial z_m} = -\frac{\partial \sigma}{\partial z_m} = -\frac{1}{p^*} \frac{\partial p}{\partial z_m} = \frac{\rho g}{p^*}. \tag{3.1.3}$$

Incorporating Equation (3.1.3) with conformal map coordinates the following expression is obtained for γ

$$\sqrt{\gamma} = \frac{1}{m^2} \frac{p^*}{\rho g} \tag{3.1.4}$$

where m is the map scale factor. Expressions of m for various conformal mapped coordinates can be found in Srivastava et al (1994).

As for the contravariant velocities, the first two components are

$$\begin{aligned} v^1 = u_m = mU \\ v^2 = v_m = mV \end{aligned} \tag{3.1.5}$$

The third velocity component, $v^3 = -\dot{\sigma}$, is obtained from the continuity equation using these two components. Note that the continuity equation (for air) in the coordinate system described above becomes:

$$\frac{\partial}{\partial t} \left(\sqrt{\gamma} \rho \right) = -\frac{\partial}{\partial x_m} \left(\sqrt{\gamma} \rho \, u_m \right) - \frac{\partial}{\partial y_m} \left(\sqrt{\gamma} \rho \, v_m \right) - \frac{\partial}{\partial \sigma} \left(\sqrt{\gamma} \rho \, \dot{\sigma} \right) \tag{3.1.6}$$

Using Equation (3.1.4) in the above and simplifying

$$\frac{\partial p^*}{\partial t} = -m^2 \left[\frac{\partial}{\partial x_m} \left(p^* \frac{U}{m} \right) + \frac{\partial}{\partial y_m} \left(p^* \frac{V}{m} \right) \right] - \frac{\partial}{\partial \sigma} \left(p^* \dot{\sigma} \right) \tag{3.1.7}$$

Using the following boundary conditions for $\dot{\sigma}$

$$\dot{\sigma} = 0 \text{ at } \sigma = 0 \text{ (at the surface) and}$$

$$\dot{\sigma} = 0 \text{ at } \sigma = 1 \text{ (at the top)} \quad,$$

one can integrate Equation (3.1.7) vertically from $\sigma = 0$ to an arbitrary σ level, to obtain $\dot{\sigma}$ from the horizontal velocities at that level,

$$\dot{\sigma} = \frac{\sigma}{p^*}\frac{\partial p^*}{\partial t} + \frac{1}{p^*}\int_0^\sigma \left\{ m^2\left[\frac{\partial}{\partial x_m}\left(p^*\frac{U}{m}\right) + \frac{\partial}{\partial y_m}\left(p^*\frac{V}{m}\right)\right]\right\}d\sigma \tag{3.1.8}$$

If this is done over the entire atmosphere (i.e., from $\sigma = 0$ to $\sigma = 1$), then the following expression is obtained:

$$\frac{\partial p^*}{\partial t} = \int_0^1 \left\{ m^2\left[\frac{\partial}{\partial x_m}\left(p^*\frac{U}{m}\right) + \frac{\partial}{\partial y_m}\left(p^*\frac{V}{m}\right)\right]\right\}d\sigma \tag{3.1.9}$$

The expression in Equation (3.1.9) can be substituted into Equation (3.1.8) and $\dot{\sigma}$ can be computed as a function of σ. Finally, assuming the slope of the terrain is shallow, i.e.,

$$\frac{\partial \sigma}{\partial x_m} << 1 \text{ and } \frac{\partial \sigma}{\partial y_m} << 1, \tag{3.1.10}$$

the contravariant diffusivities become

$$\begin{aligned} K^{11} &= m^2 K_h \\ K^{22} &= m^2 K_h \\ K^{33} &\approx \frac{\rho g}{p^*} K_v \end{aligned} \tag{3.1.11}$$

where, K_h and K_v denote the horizontal and vertical eddy diffusivities, respectively.

For hydrostatic sigma-pressure coordinates, MAQSIP solves Equation (2.3) with the above representations for $\sqrt{\gamma}$, $\overline{v^j}$, and K^{jj}.

3.2 NON-HYDROSTATIC SIGMA-PRESSURE COORDINATES

MAQSIP can be configured as a non-hydrostatic model that utilizes conformal mapping in the horizontal with sigma-pressure vertical coordinate. MAQSIP defines this coordinate system as:

$$x^1 = x_m$$
$$x^2 = y_m$$
$$x^3 = 1 - \sigma; \quad \sigma = \frac{p_0 - p_T}{p_0^*}$$

(3.2.1)

where (x_m, y_m, z_m) denote the conformal mapped coordinate system, $p_0(z_m)$ is a reference pressure, which is the horizontally averaged pressure, p_T is the pressure at the model top and is held constant, $p_0^* = p_S - p_T$, and $p_S(x_m, y_m)$ is the surface pressure at the reference state. A reference density $\rho_0(z_m)$ is defined so that the reference pressure is in hydrostatic equilibrium (Holton, 1992):

$$\frac{\partial p_0}{\partial z_m} = -\rho_0 g$$

(3.2.2)

With this definition of the coordinates, the following partial derivatives are obtained

$$\frac{\partial \sigma}{\partial x_m} = -\frac{(p_0 - p_T)}{(p_0^*)^2} \frac{\partial p_0^*}{\partial x_m} = -\frac{\sigma}{p^*} \frac{\partial p_0^*}{\partial x_m}$$
$$\frac{\partial \sigma}{\partial y_m} = -\frac{\sigma}{p_0^*} \frac{\partial p_0^*}{\partial y_m}$$
$$\frac{\partial \sigma}{\partial z_m} = \frac{1}{p_0^*} \frac{\partial p_0}{\partial z_m} = -\frac{\rho_0 g}{p_0^*}$$

(3.2.3)

Incorporating Equation (3.2.3) with conformal map coordinates the following expression is obtained for γ

$$\sqrt{\gamma} = \frac{1}{m^2} \frac{p_0^*}{\rho_0 g}$$

(3.2.4)

where m is the map scale factor. Expressions of m for various conformal mapped coordinates can be found in Srivastava et al (1994).

The first two contravariant velocity components are

$$v^1 = u_m = mU$$
$$v^2 = v_m = mV$$

(3.2.5)

while the third component is

$$v^3 = -\check{\sigma} = \frac{\sigma}{p_0^*}\left(\frac{\partial p_0^*}{\partial x_m} u_m + \frac{\partial p_0^*}{\partial y_m} v_m\right) + \frac{\rho_0 g}{p_0^*} w_m$$

(3.2.6)

$$v^3 = -\check{\sigma} = m\frac{\sigma}{p_0^*}\left(\frac{\partial p_0^*}{\partial x_m} U + \frac{\partial p_0^*}{\partial y_m} V\right) + \frac{\rho_0 g}{p_0^*} w_m$$

or,

(3.2.7)

As for the contravariant diffusivities, assuming that the terrain has a shallow slope (Pielke, 1984), i.e.,

$$\frac{\partial p_0^*}{\partial x_m} \ll 1 \quad \text{and} \quad \frac{\partial p_0^*}{\partial y_m} \ll 1$$

(3.2.9)

the following expressions are obtained

$$K^{11} \approx m^2 K_h$$
$$K^{22} \approx m^2 K_h$$
$$K^{33} \approx \frac{\rho_0 g}{p_0^*} K_v$$

(3.2.10)

where, K_h and K_v denote the horizontal and vertical eddy diffusivities, respectively.

Notice that the assumption in Equation (3.2.9) is made only for the parameterization of diffusion terms and is not applied to the contravariant velocity components in Equations (3.2.5) - (3.2.7).

For non-hydrostatic sigma-pressure coordinates, MAQSIP solves Equation (2.3) with the above representations for $\sqrt{\gamma}$, $\overline{v^j}$, and K^{ij}.

SECTION 4: COORDINATE INDEPENDENT ROUTINES

4.1 DRIVER MODULE

The **driver_ngc** module belongs to the **driver** class and contains the two main routines that control MAQSIP: DRIVER and PROCES. These two routines control the output loops, time stepping loops, and ordering of the transport, chemistry and cloud processes. These are the routines that also control the multiple grid (i.e., nesting) capabilities.

4.1.1 PROGRAM DRIVER

This is the driver for MAQSIP. It requires an input filename (HISTORY) which contains initial conditions or a restart filename from a previous run. DRIVER contains the model time stepping loop and the output loop. The following is a condensed list of function and subroutine calls.

LOGDEV = INITSCEN (PROGNAME, HISTORY, CONCFILE, STDATE, STTIME, TSTEP, NSTEPS)

CALL INCONVERT (HISTORY, CGRID, STDATE, STTIME)

CALL OUTCONVERT (CGRID, JDATE, JTIME)

DO output loop

    CALL GETSTEP (JDATE, JTIME, JTIME, MSTEP)

    DO model time loop

        CALL PROCES (CGRID, JDATE, JTIME, MSTEP)

        CALL NEXTIME (JDATE, JTIME, MSTEP)

    END DO model time loop

    CALL OUTCONVERT (CGRID, JDATE, JTIME)

END DO output loop

4.1.2 SUBROUTINE PROCES (CGRID, JDATE, JTIME, TSTEP)

Subroutine PROCES controls the ordering of the transport, chemistry and cloud processes. It is called from inside the model time loop of DRIVER. PROCES requires the latest concentration array supplied by DRIVER through the argument list. The following is a condensed list of function and subroutine calls.

IF (first time through and air is advected) THEN

CALL LOAD_DENS (CGRID, JDATE, JTIME)

ENDIF

CALL CALCMET (METRIC, METRIC_BDY, JDATE, JTIME, TSTEP)

IF (advection ordering is in the x^1, x^2, x^3 directions) THEN

CALL HADV (CGRID, METRIC, METRIC_BDY, JDATE, JTIME, TSTEP)

CALL ZADV (CGRID, METRIC, JDATE, JTIME, TSTEP)

ELSE (advection ordering is in the x^3, x^2, x^1 directions)

CALL ZADV (CGRID, METRIC, JDATE, JTIME, TSTEP)

CALL HADV (CGRID, METRIC, METRIC_BDY, JDATE, JTIME, TSTEP)

ENDIF

IF (air is advected) THEN

CALL ADJ_CON (CGRID, JDATE, JTIME, TSTEP)

END IF

CALL HDIFF (CGRID, METRIC, METRIC_BDY, JDATE, JTIME, TSTEP)

CALL VDIFF (CGRID, METRIC, JDATE, JTIME, TSTEP)

CALL DECONVERT (CGRID, JDATE, JTIME, TSTEP)

CALL CHEM (CGRID, JDATE, JTIME, TSTEP)

CALL CLDPROC (CGRID, JDATE, JTIME, TSTEP)

CALL CONVERT (CGRID, JDATE, JTIME, TSTEP)

4.2 CONVERT MODULE

The **convert_ngc** module belongs to the **couple** class and contains five routines. These routines contain unit conversions between mixing ratio units (ppm) and density units ($\mu g/m^3$). The relationship of ppm to $\mu g/m^3$ is:

$$c_{\mu g/m^3} = 1000.0_{g/kg} \cdot \rho_{kg/m^3} \cdot \frac{MW_{spc}}{MW_{air}} \cdot c_{ppm} \qquad (4.2.1)$$

Some of these routines obtain initial condition or boundary condition data from input files and do the necessary unit conversions.

4.2.1 SUBROUTINE INBDYCON (BCONC1, BCON, JDATE, JTIME)

This routine reads (and interpolates) boundary concentrations in molar mixing ratio units (ppm), converts them to density units ($\mu g/m^3$) using Equation 4.2.1, and returns the values in BCON. It requires the name of the boundary condition file which is passed through the argument list. The boundary conditions are needed in the horizontal advection and diffusion routines.

4.2.2 SUBROUTINE INCONVERT (HISTORY, CGRID, JDATE, JTIME)

This routine reads initial concentrations in molar mixing ratio units (ppm), converts them to density units ($\mu g/m^3$) using Equation 4.2.1, and returns the values in CGRID. It requires the name of the initial condition file or restart file which is passed through the argument list. The initial conditions are needed at startup. Therefore, this routine is called in the driver program before any timestepping occurs.

4.2.3 SUBROUTINE OUTCONVERT (CGRID, JDATE, JTIME)

This routine converts the concentrations CGRID (passed in through the argument list) from density units ($\mu g/m^3$) to molar mixing ratio units (ppm) using Equation 4.2.1 and writes the values to the output file. This is done every output time step in the driver.

4.2.4 SUBROUTINE CONVERT (CGRID, JDATE, JTIME, TSTEP)

This routine converts concentrations in ppm to $\mu g/m^3$ using Equation 4.2.1. Since the chemistry and cloud routines currently require ppm units, this conversion must take place in the proces routine after the cloud processor in order for the transport processes to obtain concentrations in $\mu g/m^3$.

4.2.5 SUBROUTINE DECONVERT (CGRID, JDATE, JTIME, TSTEP)

This routine converts concentrations in $\mu g/m^3$ to ppm using Equation 4.2.1. Since the chemistry and cloud routines currently require ppm units, this conversion must take place in the proces routine after all of the transport processes.

4.3 INITIALIZATION MODULE

The **init_ngc** module belongs to the **init** class and contains only one routine. This module is responsible for the initialization of MAQSIP.

4.3.1 SUBROUTINE INITSCEN (PROGNAME, HISTORY, CONCFILE, STDATE, STTIME, TSTEP, NSTEPS)

This routine initializes the unit number for the log file and reads in user input. It creates or opens the initial conditions input file (HISTORY) depending upon startup or restart status, respectively. Also, it creates or opens the output file (CONCFILE) according to the appending status of the run.

4.4 TIMESTEP MODULE

The **getstep_ngc** module belongs to the **getstep** class and only contains one routine. This module provides a timestep that assures stability given the grid spacing, the wind velocities throughout the domain and a safety factor.

4.4.1 SUBROUTINE GETSTEP (JDATE, JTIME, TSTEP, MSTEP, NREPS)

The advection time step is used as the model time step. It is computed based on the Courant-Friedrichs-Lewy (CFL) stability condition:

$$v^i \frac{\Delta t}{\Delta x^i} < 1; (i = 1, 2, 3).$$

All three directions are considered and a time step, Δt, is determined globally for the entire domain. A safety factor of $\frac{4}{3}$ is used. Therefore, the timestep is computed as:

$$\Delta t = \frac{3}{4} \min \left\{ \frac{\Delta x^1}{v^1} + \frac{\Delta x^2}{v^2} + \frac{\Delta x^3}{v^3} \right\}_{x^1, x^2, x^3}$$

Then, the time step is further adjusted such that $\Delta T/\Delta t = n$, where n is an even integer and ΔT is the output time step. This computation is repeated every ΔT. Even though the time step Δt is kept fixed for each output time step, it can vary throughout the simulation. The integer n is forced to be even so that during operator splitting in transport, the operators T_{x^1, x^2, x^3} and T_{x^3, x^2, x^1} are performed the same number of times. This insures that each time ΔT changes, the transport operators start a new sequence.

The advection modules in horizontal and vertical directions are explicit. The CFL condition must be satisfied for stability. Therefore, all three directions must be used in determining Δt.

The needed input for this routine consists of the output time step, ΔT, the date, JDATE, the time, JTIME, and the grid spacing, Δx^i. This routine obtains the required contravariant velocities associated with each cell, v^i by calling the contravariant velocity routines, HCONTVEL and VCONTVEL. It returns the timestep, Δt, and the even number of model time steps per output step.

4.5 ADVECTION MODULE

The **bot_ngc** module belongs to the **adv** class. It contains the routines that numerically solves the 3D advection process:

$$\frac{\partial}{\partial t} \left(\sqrt{\gamma} \; \overline{c_i} \right) + \frac{\partial}{\partial x^1} \left(\sqrt{\gamma} \; \overline{c_i} \; \overline{v^1} \right) + \frac{\partial}{\partial x^2} \left(\sqrt{\gamma} \; \overline{c_i} \; \overline{v^2} \right) + \frac{\partial}{\partial x^3} \left(\sqrt{\gamma} \; \overline{c_i} \; \overline{v^3} \right) = 0 \qquad (4.5.1)$$

where γ is the determinant of the metric tensor, $\overline{c_i}$ is the concentration of a particular species in mass/volume units, and $\overline{v^i}$ is the contravariant velocity in the x^i direction. The vertical coordinate, $\overline{x^3}$, is defined to be positive upward with the origin at the surface.

15

Equation (4.5.1) is solved using directional splitting (also known as time-splitting or the method of fractional steps). The solution is advanced in time as:

$$c^{n+1} = L_{x^3}(\Delta t) L_{x^2}(\Delta t) L_{x^1}(\Delta t) c^n$$

(4.5.2)

$$c^{n+2} = L_{x^1}(\Delta t) L_{x^2}(\Delta t) L_{x^3}(\Delta t) c^{n+1}$$

(4.5.3)

This module also contains a routine that attempts to correct for mass imbalances due to numerical differences between the advection schemes of the meteorology models and MAQSIP, as well as the time-splitting errors.

4.5.1   SUBROUTINE HADV (CGRID, METRIC, METRIC_BDY, JDATE, JTIME, TSTEP)

This routine solves the horizontal advection portion of the atmospheric diffusion equation.

$$\frac{\partial}{\partial t}\left(\sqrt{\gamma}\ \overline{c_i}\right) + \frac{\partial}{\partial x^1}\left(\sqrt{\gamma}\ \overline{c_i}\ \overline{v^1}\right) + \frac{\partial}{\partial x^2}\left(\sqrt{\gamma}\ \overline{c_i}\ \overline{v^2}\right) = 0$$

(4.5.4)

It orchestrates the horizontal operator splitting shown in Equations (4.5.2) and (4.5.3). The needed concentration data and the interior and boundary metric data are passed into HADV as arguments. While HADV is coordinate independent, it does call HCONTVEL for the coordinate dependent contravariant velocities. HADV also calls INBDYCON for the boundary data in the right units and ADVBOTH for the 1-D horizontal uniform grid Bott advection scheme. Outflow boundary conditions are defined by a zero slope boundary condition. Multi-dimensional data are loaded into 1-D work arrays and sent to the 1-D uniform grid Bott advection scheme.

4.5.2   SUBROUTINE ZADV (CGRID, METRIC, JDATE, JTIME, TSTEP)

This routine solves the vertical advection portion of the atmospheric diffusion equation.

$$\frac{\partial}{\partial t}\left(\sqrt{\gamma}\ \overline{c_i}\right) + \frac{\partial}{\partial x^3}\left(\sqrt{\gamma}\ \overline{c_i}\ \overline{v^3}\right) = 0$$

(4.5.5)

The needed concentration data and the interior metric data are passed into ZADV as arguments. While ZADV is coordinate independent, it does call VCONTVEL for the coordinate dependent contravariant velocities. ZADV also calls ADVBOTZ for the 1-D vertical nonuniform grid Bott advection scheme. Boundary conditions are defined by a zero flux at the surface and model top. Multi-dimensional data are loaded into 1-D work arrays and sent to the 1-D nonuniform grid Bott advection scheme.

4.5.3 SUBROUTINE ADVBOTH (NI, CON, VEL, DT, DS)

This routine implements the area-preserving flux-form advection scheme of Bott (1989ab). The scheme is positive-definite (i.e., positive fields remain positive after advection) but not monotonic (i.e., new extrema may appear after advection). As implemented in this routine, the scheme intends to solve the linear, one-dimensional advection equation:

$$\frac{\partial \psi}{\partial t} + \frac{\partial (\psi v^i)}{\partial x^i} = 0 \tag{4.5.6}$$

where $\psi(x, t)$ is a scalar field read in as CON, and v^i is the contravariant velocity read in as VEL. The values NI, DT, and DS brought in through the argument list are the number of grid cells, the time step, and the grid spacing, respectively. Here, in the horizontal advection routine, it is also assumed that the grid spacing, Δx^i_j, is constant. The flux conservative form for the advection equation is:

$$\psi^{n+1}_j = \psi^n_j - \frac{\Delta t}{\Delta x^i_j} \left[F_{j+1/2} - F_{j-1/2} \right] \tag{4.5.7}$$

The net flux through the right boundary of the grid cell j can be written as

$$F_{j+1/2} = F^+_{j+1/2} - F^-_{j+1/2} \tag{4.5.8}$$

where $F^+_{j+1/2}$ is the outflux from cell j through its right boundary and $F^-_{j+1/2}$ is the outflux from cell $j+1$ through its left boundary. The distribution of the advected quantity within the cell is represented by a polynomial of order l as:

$$\psi_{j,l}(\xi) = \sum_{k=0}^{l} a_{j,k} \xi^k \tag{4.5.9}$$

17

where $\xi = (x - x_j)/\Delta x_{\cdot j}$ Note that $\psi_j(0)$ is not necessarily equal to ψ_j. The polynomial can be made area-preserving by requiring:

$$\psi_j^n = \int_{i-1/2}^{i+1/2} \sum_{k=0}^{l} a_{j,k} \xi^k d\xi, \qquad i = 0, \pm 1, \pm 2, \dots \qquad (4.5.10)$$

Solution to this linear system yields the coefficients $a_{j,k}$, which, for horizontal advection, are for uniform grid spacing.

Here, a fourth-order polynomial (quartic) is used to represent distribution of the advected field. For a quartic (uniform grid spacing), the coefficients are as follows:

$$a_{j,0} = \frac{1}{1920} \left(9\psi_{j-2}^n - 116\psi_{j-1}^n + 2134\psi_j^n - 116\psi_{j+1}^n + 9\psi_{j+2}^n \right)$$

$$a_{j,1} = \frac{1}{48} \left(5\psi_{j-2}^n - 34\psi_{j-1}^n + 34\psi_{j+1}^n - 5\psi_{j+2}^n \right)$$

$$a_{j,2} = \frac{1}{16} \left(-\psi_{j-2}^n + 12\psi_{j-1}^n - 22\psi_j^n + 12\psi_{j+1}^n - \psi_{j+2}^n \right) \qquad (4.5.11)$$

$$a_{j,3} = \frac{1}{12} \left(-\psi_{j-2}^n + 2\psi_{j-1}^n - 2\psi_{j+1}^n + \psi_{j+2}^n \right)$$

$$a_{j,4} = \frac{1}{24} \left(\psi_{j-2}^n - 4\psi_{j-1}^n + 6\psi_j^n - 4\psi_{j+1}^n + \psi_{j+2}^n \right)$$

Note that two neighboring cells are needed at each side of the cell for this representation. Near the boundary, the representation is first changed to a second-order polynomial (quadratic) and finally to a first-order polynomial (linear). For a quadratic (uniform grid spacing), the coefficients are as follows:

$$a_{j,0} = \frac{1}{24} \left(-\psi_{j-1}^n + 26\psi_j^n - \psi_{j+1}^n \right)$$

$$a_{j,1} = \frac{1}{2} \left(-\psi_{j-1}^n + \psi_{j+1}^n \right) \qquad (4.5.12)$$

$$a_{j,2} = \frac{1}{2} \left(\psi_{j-1}^n - 2\psi_j^n + \psi_{j+1}^n \right)$$

and finally, for a first-order polynomial (uniform grid spacing) the following coefficients are used:

$$a_{j,0} = \psi_j^n$$

$$a_{j,1} = \begin{cases} -\psi_{j-1}^n + \psi_j^n \\ -\psi_j^n + \psi_{j+1}^n \end{cases}$$

(4.5.13)

Depending on which side of the domain the boundary is at, one of the expressions for $a_{j,1}$ in Equation (4.5.13) is selected.

By integrating the polynomial of Equation (4.5.9) between appropriate limits, we arrive to the following expressions for the fluxes in Equation (4.5.8).

$$F_{j+1/2}^+ = \frac{\Delta x_j^i}{\Delta t} \int_{1/2-c_j^+}^{1/2} \Psi_j(\xi) d\xi$$

$$F_{j-1/2}^- = \frac{\Delta x_j^i}{\Delta t} \int_{-1/2}^{-1/2+c_{j-1}^-} \Psi_j(\xi) d\xi$$

(4.5.14)

where

$$c_j^{\pm} = \pm \frac{\Delta t}{2\Delta x_j^i} \left(v_{j\pm1/2}^i \pm \left| v_{j\pm1/2}^i \right| \right)$$

(4.5.15)

Finally, to make the scheme positive-definite, the total outflux from the cell j is limited by requiring that

$$0 \leq F_{j+1/2}^+ + F_{j-1/2}^- \leq \frac{\Delta x_j^i}{\Delta t} \psi_j^n$$

(4.5.16)

The numerical procedure for each cell j is as follows:

- Compute the coefficients of the area-preserving polynomial, $a_{j,k}$

- Integrate this polynomial to compute the fluxes coming in or out of the cell

- Normalize fluxes so that the outflux from a cell is limited according to Equation (4.5.16)

- Compute advected field using the flux-form of Equation (4.5.7)

4.5.4 SUBROUTINE ADVBOTZ (NI, CON, VEL, DT, DS)

This routine also implements the positive-definite area-preserving flux-form advection scheme of Bott (1989ab). It intends to solve the linear, one-dimensional advection equation:

$$\frac{\partial \psi}{\partial t} + \frac{\partial \left(\psi v^3\right)}{\partial x^3} = 0 \tag{4.5.17}$$

where $\psi(x, t)$ is a scalar field read in as CON, and v^3 is the contravariant velocity read in as VEL. The values NI, DT, and DS brought in through the argument list are the number of grid cells, the time step, and the grid spacing, respectively. The largest difference of the vertical Bott scheme from the horizontal, is that the grid spacing, Δx_j^3, does not need to be constant.

Here, a second-order polynomial (quadratic) is used to represent distribution of the advected field. For a quadratic (nonuniform grid distribution), the coefficients are as follows:

$$a_{j,0} = \psi_j^n - \frac{1}{4} \frac{T_{j,1} + T_{j,2}}{T_{j,0}} \left(\Delta x_j^3\right)^2$$

$$a_{j,1} = \frac{T_{j,1}\left(\Delta x_j^3 + 2\Delta x_{j-1}^3\right) - T_{j,2}\left(\Delta x_j^3 + 2\Delta x_{j+1}^3\right)}{T_{j,0}} \Delta x_j^3 \tag{4.5.18}$$

$$a_{j,2} = 3 \frac{\left(T_{j,1} + T_{j,2}\right)}{T_{j,0}} \left(\Delta x_j^3\right)^2$$

where,

$$T_{j,0} = \left(\Delta x_j^3 + \Delta x_{j-1}^3\right)\left(\Delta x_j^3 + \Delta x_{j+1}^3\right)\left(\Delta x_{j-1}^3 + \Delta x_j^3 + \Delta x_{j+1}^3\right)$$

$$T_{j,1} = \left(\Delta x_j^3 + \Delta x_{j-1}^3\right)\left(\Psi_{j+1}^n - \Psi_j^n\right)$$

$$T_{j,2} = \left(\Delta x_j^3 + \Delta x_{j+1}^3\right)\left(\Psi_{j-1}^n - \Psi_j^n\right)$$

Note that only one neighboring cell is needed at each side of the cell for this representation. Also, note that when grid spacing is uniform, Equation (4.5.18) reduces to Equation (4.5.12).

Near the boundary, the representation is changed to a first-order polynomial (linear). The first-order polynomial (nonuniform grid distribution) coefficients are:

$$a_{j,0} = \psi_j^n$$

$$a_{j,1} = \begin{cases} \dfrac{2\Delta x_j^3}{\left(\Delta x_j^3 + \Delta x_{j-1}^3\right)}\left(\psi_j^n - \psi_{j-1}^n\right) \\[2em] \dfrac{2\Delta x_j^3}{\left(\Delta x_j^3 + \Delta x_{j+1}^3\right)}\left(\psi_{j+1}^n - \psi_j^n\right) \end{cases} \qquad (4.5.19)$$

Depending on which side of the domain the boundary is at, one of the expressions for $a_{j,1}$ in Equation (4.5.19) is selected. These relationships reduce to the uniform grid relationships of Equation (4.5.13) with uniform grid spacing. With the exception of the change of the coefficients for the polynomials, the vertical Bott scheme is implemented the same way as the horizontal Bott scheme.

21

4.5.5 SUBROUTINE ADJ_CON (CGRID, JDATE, JTIME, TSTEP)

This routine attempts to correct for mass imbalances due to numerical indifferences between the advection schemes of the meteorology preprocessors and MAQSIP. Density values are the only input to this routine other than the passed arguments. It adjusts the concentration field (if desired) as follows:

$$c_j^{adj} = c_j^{adv} \frac{\rho_j^{int}}{\rho_j^{adv}} \tag{4.5.20}$$

where c_j^{adj} is adjusted concentration, ρ_j^{adv} advected air density, and ρ_j^{int} interpolated air density. ADJ_CON is called from PROCES after each advection step.

This procedure is implemented by adding air density to the list of advected species. Air acts as a tracer gas which is advected (and only advected) along with the other species. After the advection step is completed, the concentrations of all the species are adjusted according to the variance of the tracer gas from the known interpolated values. This is accomplished by Equation (4.5.20). To start the procedure, another routine, LOAD_DENS is used to load the initial density values into the concentration array. All subsequent interpolations of density are performed in ADJ_CON.

4.6 DIFFUSION MODULE

The **eddy_ngc** module belongs to the **diff** class. It contains the routines that numerically solves the 3-D diffusion process:

$$\frac{\partial}{\partial t}\left[\sqrt{\gamma}\,c\right] = \frac{\partial}{\partial x^1}\left[\sqrt{\gamma}\rho K^{11}\frac{\partial}{\partial x^1}\left[\frac{c}{\rho}\right]\right] + \frac{\partial}{\partial x^2}\left[\sqrt{\gamma}\rho K^{22}\frac{\partial}{\partial x^2}\left[\frac{c}{\rho}\right]\right]$$

$$+ \frac{\partial}{\partial x^3}\left[\sqrt{\gamma}\rho K^{33}\frac{\partial}{\partial x^3}\left[\frac{c}{\rho}\right]\right] + \sqrt{\gamma}\,S$$

where γ is the determinant of the metric tensor, c is the concentration of a particular species in density units, and K^{ii} are the contravariant diffusivities in the x^i direction, ρ is the air density, and S is the emission source term. The vertical coordinate, x^3 is defined to be positive upward with the origin at the surface. The input to these routines are listed in Section 7.2.

4.6.1   SUBROUTINE HDIFF (CGRID, METRIC, METRIC_BDY, JDATE, JTIME, TSTEP)

This subroutine solves the equation:

$$\frac{\partial}{\partial t}\left[\sqrt{\gamma}\,c\right] = \frac{\partial}{\partial x^1}\left[\sqrt{\gamma}\rho K^{11}\frac{\partial}{\partial x^1}\left[\frac{c}{\rho}\right]\right] + \frac{\partial}{\partial x^2}\left[\sqrt{\gamma}\rho K^{22}\frac{\partial}{\partial x^2}\left[\frac{c}{\rho}\right]\right] \qquad (4.6.1)$$

where c is the concentration in mass/volume units ($\mu g/m^3$), γ is the determinant of the metric tensor, x^1 and x^2 are the horizontal coordinates, ρ is the density, and K^{11} and K^{22} are the horizontal contravariant diffusivities. The routine itself is general for all coordinate systems. However, it calls a coordinate-dependent subroutine, HCONTDIFF, that provides the horizontal contravariant diffusivities. Other routines called by HDIFF are HCONTVEL and INBDYCON which provide the horizontal contravariant velocities and the boundary concentrations ($\mu g/m^3$), respectively.

4.6.2   SUBROUTINE VDIFF (CGRID, METRIC, JDATE, JTIME, TSTEP)

This subroutine is the vertical diffusion component and solves the following equation:

$$\frac{\partial}{\partial t}\left[\sqrt{\gamma}\,c\right] = \frac{\partial}{\partial x^3}\left[\sqrt{\gamma}\rho K^{33}\frac{\partial}{\partial x^3}\left[\frac{c}{\rho}\right]\right] + \sqrt{\gamma}S \qquad (4.6.2)$$

where x^3 is the vertical coordinate, K^{33} is the contravariant diffusivity in the x^3-direction and S is the emission source term. A detailed derivation of Equation (4.6.2) can be found in Srivastava et al (1994).

The following boundary conditions are used for solving Equation (4.6.2). At the surface:

$$\sqrt{\gamma}\rho K^{33}\frac{\partial}{\partial x^3}\left[\frac{c}{\rho}\right] = \sqrt{\gamma}\,v_{dep}^3\,c \qquad (4.6.3)$$

where v_{dep}^3 is the deposition velocity (positive in the negative x^3-direction). At the top of the model:

$$\frac{\partial}{\partial x^3}\left[\frac{c}{\rho}\right] = 0 \qquad (4.6.4)$$

It is also important to recall that while c and ρ are defined at layer midpoints, K^{33} is defined at the boundary between two layers as explained in the documentation for subroutine EDYINTB.

To describe the numerical procedure, it is useful to define a diffusive flux term F^D

$$F^D = -\sqrt{\gamma}\rho K^{33}\frac{\partial}{\partial x^3}\left[\frac{c}{\rho}\right] \qquad (4.6.5)$$

Now, Equation (4.6.2) can be rewritten as:

$$\frac{\partial}{\partial t}\left[\sqrt{\gamma}\,c\right] = \frac{\partial}{\partial x^3}\left[-F^D\right] + \sqrt{\gamma}S \qquad (4.6.6)$$

For time-stepping the following general time integration formula is used

$$\frac{\left(\sqrt{\gamma}c\right)^{n+1} - \left(\sqrt{\gamma}c\right)^{n}}{\Delta t} = \theta\left(\frac{\partial}{\partial t}\left[\sqrt{\gamma}c\right]\right)^{n+1} + [1-\theta]\left(\frac{\partial}{\partial t}\left[\sqrt{\gamma}c\right]\right)^{n} \qquad (4.6.7)$$

It should be noted that the error term in Equation (4.6.7) is, in general, of the order of Δt, i.e., the formula is first-order accurate. There are three special cases that are worth mentioning: first, when $\theta=0$, the formula is explicit. Second, when $\theta=1$, the formula is fully implicit. Finally, when $\theta=1/2$, Equation (4.6.7) becomes the second-order accurate Crank-Nicolson time integration scheme. Currently, the Crank-Nicolson integration is being implemented in this subroutine, but this can be changed by simply altering the value of the parameter θ. It is important to notice that all time dependent variables other than the concentration, c, are evaluated at the middle of the model time step. We will denote this with the use of superscript $N+1/2$ here, with N representing the model time-level as opposed to n, which represents the process time level.
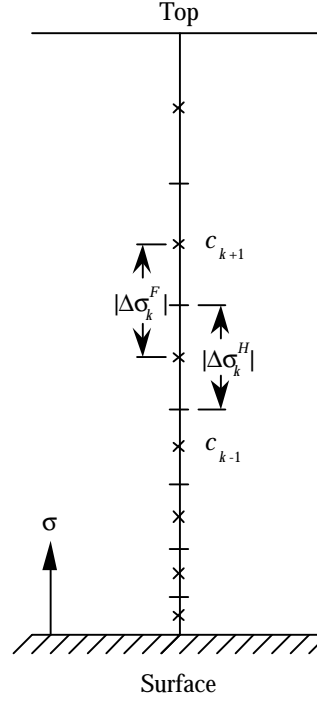
Figure 4.1. Definition of the x^3-coordinate system (x^3 denoted, in this section, by σ)

The stencil in Figure 4.1 illustrates the notation in the rest of this document. Note that we are denoting x^3 by σ hereafter. This should not be confused with σ in other sections which define σ as downward from he top of the model. The spatial approximation used for the right-hand-side of Equation (4.6.6) is the second-order accurate central differencing:

$$\left(\frac{\partial}{\partial \sigma}\left[F^D\right]\right)_k = \frac{\left(F^D\right)_{k+1/2} - \left(F^D\right)_{k-1/2}}{\left(\Delta\sigma^H\right)_k} + O\!\left[\left(\Delta\sigma^H\right)_k^2\right] \qquad (4.6.8)$$

Recall the definition of the diffusive flux in Equation (4.6.5). Using central differencing one more time to express the derivative term at the boundary between two layers we get:

$$\left(F^D\right)_{k+1/2} = -\left(\sqrt{\gamma}\rho K^{33}\right)_{k+1/2} \frac{(c/\rho)_{k+1} - (c/\rho)_k}{\left(\Delta\sigma^F\right)_k} \qquad (4.6.9)$$

Equation (4.6.9) is second-order accurate only if the grid is uniform. When grid spacing is not uniform, one cannot say that the accuracy of this formula is second order. Finally, the substitution of Equations (4.6.8 - 4.6.9) into Equation (4.6.7) yields

$$\left(\sqrt{\gamma}\right)_k^{N+1/2} \frac{(c)_k^{n+1} - (c)_k^n}{\Delta t} = \frac{\theta}{\left(\Delta\sigma^H\right)_k}\left[\left(\sqrt{\gamma}\rho K^{33}\right)_{k+1/2}^{N+1/2} \frac{(c)_{k+1}^{n+1}/(\rho)_{k+1}^{N+1/2} - (c)_k^{n+1}/(\rho)_k^{N+1/2}}{\left(\Delta\sigma^F\right)_k}\right.$$

$$\left. -\left(\sqrt{\gamma}\rho K^{33}\right)_{k-1/2}^{N+1/2} \frac{(c)_k^{n+1}/(\rho)_k^{N+1/2} - (c)_{k-1}^{n+1}/(\rho)_{k-1}^{N+1/2}}{\left(\Delta\sigma^F\right)_{k-1}}\right]$$

$$+\frac{1-\theta}{\left(\Delta\sigma^H\right)_k}\left[\left(\sqrt{\gamma}\rho K^{33}\right)_{k+1/2}^{N+1/2} \frac{(c)_{k+1}^n/(\rho)_{k+1}^{N+1/2} - (c)_k^n/(\rho)_k^{N+1/2}}{\left(\Delta\sigma^F\right)_k}\right.$$

$$\left. -\left(\sqrt{\gamma}\rho K^{33}\right)_{k-1/2}^{N+1/2} \frac{(c)_k^n/(\rho)_k^{N+1/2} - (c)_{k-1}^n/(\rho)_{k-1}^{N+1/2}}{\left(\Delta\sigma^F\right)_{k-1}}\right] \quad (4.6.10)$$

$$+\left(\sqrt{\gamma}S\right)_k^{N+1/2}$$

which can also be written in the following tridiagonal form:

$$\left[\frac{\left(\sqrt{\gamma}\right)_k^{N+1/2}}{\Delta t} + \frac{\theta}{\left(\Delta\sigma^H\right)_k}\left[\left(\sqrt{\gamma}\rho K^{33}\right)_{k+1/2}^{N+1/2} \frac{1/(\rho)_k^{N+1/2}}{\left(\Delta\sigma^F\right)_k} + \left(\sqrt{\gamma}\rho K^{33}\right)_{k-1/2}^{N+1/2} \frac{1/(\rho)_k^{N+1/2}}{\left(\Delta\sigma^F\right)_{k-1}}\right]\right](c)_k^{n+1}$$

$$-\frac{\theta}{\left(\Delta\sigma^H\right)_k}\left(\sqrt{\gamma}\rho K^{33}\right)_{k-1/2}^{N+1/2} \frac{1/(\rho)_{k-1}^{N+1/2}}{\left(\Delta\sigma^F\right)_{k-1}}(c)_{k-1}^{n+1} - \frac{\theta}{\left(\Delta\sigma^H\right)_k}\left(\sqrt{\gamma}\rho K^{33}\right)_{k+1/2}^{N+1/2} \frac{1/(\rho)_{k+1}^{N+1/2}}{\left(\Delta\sigma^F\right)_k}(c)_{k+1}^{n+1} =$$

$$\left[\frac{\left(\sqrt{\gamma}\right)_k^{N+1/2}}{\Delta t} - \frac{1-\theta}{\left(\Delta\sigma^H\right)_k}\left[\left(\sqrt{\gamma}\rho K^{33}\right)_{k+1/2}^{N+1/2} \frac{1/(\rho)_k^{N+1/2}}{\left(\Delta\sigma^F\right)_k} + \left(\sqrt{\gamma}\rho K^{33}\right)_{k-1/2}^{N+1/2} \frac{1/(\rho)_k^{N+1/2}}{\left(\Delta\sigma^F\right)_{k-1}}\right]\right](c)_k^n$$

$$+\frac{1-\theta}{\left(\Delta\sigma^H\right)_k}\left(\sqrt{\gamma}\rho K^{33}\right)_{k-1/2}^{N+1/2} \frac{1/(\rho)_{k-1}^{N+1/2}}{\left(\Delta\sigma^F\right)_{k-1}}(c)_{k-1}^n + \frac{1-\theta}{\left(\Delta\sigma^H\right)_k}\left(\sqrt{\gamma}\rho K^{33}\right)_{k+1/2}^{N+1/2} \frac{1/(\rho)_{k+1}^{N+1/2}}{\left(\Delta\sigma^F\right)_k}(c)_{k+1}^n \quad (4.6.11)$$

$$+\left(\sqrt{\gamma}S\right)_k^{N+1/2}$$

Notice that all time dependent variables other than the concentration c are evaluated at the middle of the model time step, $N+1/2$. Also recall that although the vertical diffusivities are defined at the boundary between two layers, the densities and metrics are defined at the layer midpoints. Therefore:

$$\left(\sqrt{\gamma}\rho K^{33}\right)_{k+1/2} = \left[\frac{\left(\sqrt{\gamma}\rho\right)_{k+1} + \left(\sqrt{\gamma}\rho\right)_k}{2}\right]\left(K^{33}\right)_{k+1/2} \quad (4.6.12)$$

This is the system of equations being implemented in the subroutine for $k=2,...,KMAX-1$. The bottom boundary condition in Equation (4.6.3) is applied in the following way:

$$\left(\sqrt{\gamma}\rho K^{33}\right)^{N+1/2}_{1/2}\frac{(c)_1/(\rho)_1^{N+1/2}-(c)_0/(\rho)_0^{N+1/2}}{\left(\Delta\sigma^F\right)_0}=\left(\sqrt{\gamma}\right)^{N+1/2}_{1/2}\left(v^3_{dep}\right)^{N+1/2}c_1 \qquad (4.6.13)$$

which results in the first equation of the system:

$$\left[\frac{\left(\sqrt{\gamma}\right)_1^{N+1/2}}{\Delta t}+\frac{\theta}{\left(\Delta\sigma^H\right)_1}\left[\left(\sqrt{\gamma}\rho K^{33}\right)^{N+1/2}_{3/2}\frac{1/(\rho)_1^{N+1/2}}{\left(\Delta\sigma^F\right)_1}+\left(\sqrt{\gamma}\right)^{N+1/2}_{1/2}\left(v^3_{dep}\right)^{N+1/2}\right]\right](c)_1^{n+1}$$

$$-\frac{\theta}{\left(\Delta\sigma^H\right)_1}\left(\sqrt{\gamma}\rho K^{33}\right)^{N+1/2}_{3/2}\frac{1/(\rho)_2^{N+1/2}}{\left(\Delta\sigma^F\right)_1}(c)_2^{n+1}=$$

$$\left[\frac{\left(\sqrt{\gamma}\right)_1^{N+1/2}}{\Delta t}-\frac{1-\theta}{\left(\Delta\sigma^H\right)_1}\left[\left(\sqrt{\gamma}\rho K^{33}\right)^{N+1/2}_{3/2}\frac{1/(\rho)_1^{N+1/2}}{\left(\Delta\sigma^F\right)_1}-\left(\sqrt{\gamma}\right)^{N+1/2}_{1/2}\left(v^3_{dep}\right)^{N+1/2}\right]\right](c)_1^{n} \qquad (4.6.14)$$

$$+\frac{1-\theta}{\left(\Delta\sigma^H\right)_1}\left(\sqrt{\gamma}\rho K^{33}\right)^{N+1/2}_{3/2}\frac{1/(\rho)_2^{N+1/2}}{\left(\Delta\sigma^F\right)_1}(c)_2^{n}+\left(\sqrt{\gamma}S\right)^{N+1/2}_1$$

The emissions source term in Equation (4.6.14) has units of $\frac{\mu g}{m^3 s}$. However, the emission data contained in the input file has units of $\frac{g}{s}$. Therefore, the source term is divided by the cell volume $(V=\sqrt{\gamma}\Delta x^1\Delta x^2\Delta x^3)$ and multiplied by 10^6 (to convert from g to μg) in order to obtain the correct units: e.g.,

$$\sqrt{\gamma}S=\frac{EMIS_{input}10^6}{\Delta x^1\Delta x^2\Delta x^3}$$

The boundary condition at the top of the atmosphere is applied as follows:

$$\left(\sqrt{\gamma}\rho K^{33}\right)^{N+1/2}_{KMAX+1/2}\frac{(c)_{KMAX+1}/(\rho)_{KMAX+1}^{N+1/2}-(c)_{KMAX}/(\rho)_{KMAX}^{N+1/2}}{\left(\Delta\sigma^F\right)_{KMAX}}=0 \qquad (4.6.15)$$

which results in the last equation of the system:

$$
\left[\frac{\left(\sqrt{\gamma}\right)^{N+1/2}_{KMAX}}{\Delta t} + \frac{\theta}{\left(\Delta\sigma^{H}\right)_{KMAX}}\left[\left(\sqrt{\gamma}\rho K^{33}\right)^{N+1/2}_{KMAX-1/2}\frac{1\!\!/\left(\rho\right)^{N+1/2}_{KMAX}}{\left(\Delta\sigma^{F}\right)_{KMAX-1}}\right]\right](c)^{n+1}_{KMAX}
$$

$$
-\frac{\theta}{\left(\Delta\sigma^{H}\right)_{KMAX}}\left(\sqrt{\gamma}\rho K^{33}\right)^{N+1/2}_{KMAX-1/2}\frac{1\!\!/\left(\rho\right)^{N+1/2}_{KMAX-1}}{\left(\Delta\sigma^{F}\right)_{KMAX-1}}(c)^{n+1}_{KMAX-1} =
$$

$$
\left[\frac{\left(\sqrt{\gamma}\right)^{N+1/2}_{KMAX}}{\Delta t} - \frac{1-\theta}{\left(\Delta\sigma^{H}\right)_{KMAX}}\left[\left(\sqrt{\gamma}\rho K^{33}\right)^{N+1/2}_{KMAX-1/2}\frac{1\!\!/\left(\rho\right)^{N+1/2}_{KMAX}}{\left(\Delta\sigma^{F}\right)_{KMAX-1}}\right]\right](c)^{n}_{KMAX} \qquad (4.6.16)
$$

$$
+\frac{1-\theta}{\left(\Delta\sigma^{H}\right)_{KMAX}}\left(\sqrt{\gamma}\rho K^{33}\right)^{N+1/2}_{KMAX-1/2}\frac{1\!\!/\left(\rho\right)^{N+1/2}_{KMAX-1}}{\left(\Delta\sigma^{F}\right)_{KMAX-1}}(c)^{n}_{KMAX-1} + \left(\sqrt{\gamma}S\right)^{N+1/2}_{KMAX}
$$

This tridiagonal system of equations (i.e., Equations 4.6.11, 4.6.14, and 4.6.16) are solved using the Thomas algorithm.

VDIFF calls two coordinate-dependent subroutines, VCONTDIFF and DEPCONTVEL that provide the vertical contravariant diffusivity and contravariant deposition velocities, respectively.

4.6.3 SUBROUTINE EDYINTB (EDDYV, DT, JDATE, JTIME, TSTEP)

This routine computes the contravariant vertical eddy diffusivity (EDDYV) for VDIFF using the integrated version of the Heinz formula by Byun (19xx). It also estimates the characteristic diffusion time step (DT) with a built in safety factor. This routine itself is general for all coordinate systems. However, it calls HEIGHT, a coordinate dependent routine, to obtain the cell-heights values.

4.6.4 SUBROUTINE TRIDIAG (A, B, E, D, U)

This routine solves the resulting tridiagonal system of VDIFF using the Thomas algorithm [Anderson et al, 1984]. *A*, *B*, and *E* are the lower diagonal, diagonal, and upper diagonal vectors, respectively. *D* is the right hand side vector. *U* is the solution vector.

4.7 CHEMISTRY MODULES

The only coordinate dependence in the chemistry modules is a cell-height calculation needed to interpolate photolytic data. This dependence is eliminated by calling a coordinate dependent module which produces the heights for whatever coordinate system is being used. There are currently two chemistry mechanisms built for MAQSIP. They both belong to the **chem** class. The RADM2 Chemistry Mechanism, located in the **radm2_mqssa_ngc** module, implements the mechanism by Stockwell et al (1990). The CB4 Chemistry Mechanism, located in the **cb4_ngc** module, implements the mechanism by Gery et al (1989).

4.8 CLOUD MODULES

Like the chemistry modules, the only coordinate dependence in the chemistry modules is a cell-height calculation needed to interpolate photolytic data. This dependence is eliminated by calling a coordinate dependent module which produces the heights for whatever coordinate system is being used. Currently, only one cloud mechanism is built for MAQSIP. It belongs to the **cloud** class. It is the RADM cloud mechanism (Chang et al, 1987) which is located in the **radm_cloud_ngc** module. The CB4 cloud mechanism, which would be located in the **cb4_cloud_ngc** module in a future version, has not been created.

SECTION 5: COORDINATE DEPENDENT ROUTINES

5.1 COORDINATE MODULES

Currently, two vertical coordinate systems are supported by MAQSIP. They are the hydrostatic sigma-pressure coordinate system (RADM-type) and the non-hydrostatic sigma-pressure coordinate system (SAQM-type). Both of these coordinate systems have Lambert conformal mapping in the horizontal plane.

Coordinate dependent variables have been separated out of the governing equations and grouped together into a module of their own. For example, the contravariant velocity is directly associated with the coordinate system the equations are solved in. Therefore, the contravariant velocity calculation belongs to a coordinate module.

A coordinate module is created for each coordinate system for which MAQSIP can be solved and placed into the **coord** class. Currently, two coordinate modules that have been created: **sigma_p_hyd** (RADM-type) and **sigma_p_nhy** (SAQM-type). While each coordinate module contains the same set of seven routines, each routine computes data for its own coordinate system. The seven coordinate dependent data needed are: 1) the determinant of the metric tensor, $\sqrt{\gamma}$, 2) the cell height, 3) the horizontal contravariant velocities, 4) the vertical contravariant velocities, v^j, 5) the horizontal contravariant diffusivities, 6) the vertical contravariant diffusivities, K^{jj}, and 7) the contravariant deposition velocity. The methods used in obtaining this data are described below.

5.1.1 SUBROUTINE CALCMET (METRIC, METRIC_BDY, JDATE, JTIME, TSTEP)

This subroutine computes $\sqrt{\gamma}$ for the interior (METRIC) and the boundary (METRIC_BDY) of the modeling domain. For the RADM-type coordinate system,

$$\sqrt{\gamma} = \frac{1}{m^2} \frac{p^*}{\rho g}$$

where, $m(x^1, y^2)$ is the map factor for Lambert conformal map coordinates, $p^* = p_S - p_T$, $p_S(x^1, x^2, t)$ is the surface pressure, p_T is the pressure at the model top and is held constant, and $\rho(x^1, x^2, \sigma, t)$ is the density.

For the SAQM-type coordinate system,

$$\sqrt{\gamma} = \frac{1}{m^2} \frac{p_0^*}{\rho_0 g}$$

where, $p_0^* = p_S - p_T$, $p_S(x^1, x^2)$ is the surface pressure at the reference state and $\rho_0(x^1, x^2, \sigma)$ is defined so that the reference pressure is in hydrostatic equilibrium (Holton, 1992).

5.1.2 SUBROUTINE HEIGHT (ZH, ZF, JDATE, JTIME, TSTEP)

This subroutine reads in the cell height for modeling domain from an input file. These height values are different for each of the two current coordinate systems. For the RADM-type coordinate system the half-level heights (ZH) and the full-level heights (ZF) are time dependent. However, for the SAQM-type coordinate system, these values remain constant in time.

5.1.3   SUBROUTINE HCONTVEL (UWIND, VWIND, JDATE, JTIME, TSTEP)

This routine computes the horizontal contravariant velocities, $\overline{v^1}$ and $\overline{v^2}$, and depends on the coordinate system. For Lambert Conformal Map coordinates, the contravariant velocities are:

$$v^1 = mU$$
$$v^2 = mV$$

where U and V are the rotated physical velocities. Note that this routine is the same for RADM- and SAQM-type coordinates since both use Lambert conformal map coordinates in the horizontal plane.

5.1.4 SUBROUTINE VCONTVEL (WWIND, JDATE, JTIME, TSTEP)

This routine computes the vertical contravariant velocity, v^3. For the RADM-type coordinate system,

$$\frac{\partial p^*}{\partial t} = -m^2 \left[\frac{\partial}{\partial x_m} \left(p^* \frac{U}{m} \right) + \frac{\partial}{\partial y_m} \left(p^* \frac{V}{m} \right) \right] - \frac{\partial}{\partial \sigma} (p^* \dot{\sigma})$$

The boundary conditions on the vertical velocity $\dot{\sigma} = d\sigma/dt$ are:

$$\dot{\sigma} = 0 \text{ at } \sigma = 0 \text{ (at the surface)}$$

$$\dot{\sigma} = 0 \text{ at } \sigma = 1 \text{ (at the top)}$$

This equation is integrated vertically from $\sigma = 0$ to an arbitrary σ level, to obtain $\dot{\sigma}$ from the horizontal velocities at that level,

$$\dot{\sigma} = \frac{\sigma}{p^*} \frac{\partial p^*}{\partial t} + \frac{1}{p^*} \int_0^\sigma \left\{ m^2 \left[\frac{\partial}{\partial x_m} \left(p^* \frac{U}{m} \right) + \frac{\partial}{\partial y_m} \left(p^* \frac{V}{m} \right) \right] \right\} d\sigma$$

This is done over the entire atmosphere (i.e., from $\sigma = 0$ to $\sigma = 1$) and the following expression is obtained:

$$\frac{\partial p^*}{\partial t} = \int_0^1 \left\{ m^2 \left[\frac{\partial}{\partial x_m} \left(p^* \frac{U}{m} \right) + \frac{\partial}{\partial y_m} \left(p^* \frac{V}{m} \right) \right] \right\} d\sigma.$$

Then this expression is substituted into the above equation for $\dot{\sigma}$, yielding an calculation of $\dot{\sigma}$ as a function of σ.

For the SAQM-type coordinate system,

$$v^3 = -\dot{\sigma}; \dot{\sigma} = \frac{\sigma}{p_0^*} \left(\frac{\partial p_0^*}{\partial x^1} v^1 + \frac{\partial p_0^*}{\partial x^2} v^2 \right) + \frac{\rho_0 g}{p_0^*} w$$

where w is the physical vertical velocity.

For both coordinate systems, the horizontal contravariant velocities are obtained through a call to HCONTVEL.

5.1.5 SUBROUTINE HCONTDIFF (ALLK11, ALLK22, JDATE, JTIME)

This routine computes the horizontal contravariant diffusivities, K^{11} and K^{22}. For Lambert conformal map coordinates, the contravariant diffusivities are:

$$K^{11} = m^2 K_h$$
$$K^{22} = m^2 K_h$$

where K_h is the physical horizontal diffusivity (parameterized).

Note that this routine is the same for RADM- and SAQM-type coordinates since both use Lambert conformal map coordinates in the horizontal plane.

5.1.6 SUBROUTINE VCONTDIFF (EDDYV, DT, JDATE, JTIME, TSTEP)

This routine computes the vertical contravariant diffusivity, K^{33}. For the RADM-type coordinate system,

$$K^{33} = \left(\frac{\rho g}{p^*} \right) K_v$$

where K_v is the physical vertical diffusivity (parameterized).

For the SAQM-type coordinate system,

$$K^{33} = \left(\frac{\rho_0 g}{p_0^*} \right) K_v$$

5.1.7 SUBROUTINE DEPCONTVEL (VDEP, JDATE, JTIME, TSTEP)

This routine computes the contravariant deposition velocity, v_{dep}^3. For the RADM-type coordinate system,

$$v_{dep}^3 = \frac{\rho g}{p^*} v_{dep}$$

34

where v_{dep} is the physical deposition velocity. For the SAQM-type coordinate system,

$$v_{dep}^3 = \frac{\rho_0 g}{p_0^*} v_{dep}$$

SECTION 6: REQUIRED EXTERNAL INCLUDE FILES

6.1 IOAPI DECLARATIONS

There are three Fortran include files needed from the I/O API: **PARMS3.EXT, FDESC3.EXT,** and **IODECL3.EXT.** Each include file is well documented both in the files and on-line at `/pub/storage/xcc/work/m3io/H.INCLUDE.html`. These files can be found in `/pub/storage/edss/aqm/src/icl/m3io` on the EPA research subnetworkstations and in `/usr/local/edss/aqm/src/icl/m3io` on *flyer* and *sequoia*.

6.2 NEEDED CONSTANTS

There is an include file which defines the needed constants for MAQSIP: **CONST3.EXT**. This file can be obtained from *sams* from the module *shared*.

6.3 I/O FILE DECLARATIONS

The input and output filenames must be defined for each grid domain. These filenames are defined in files named **FILES3_G*.EXT**. The "*****" signifies the number denoting a unique grid domain (e.g., 0, 1, 11, 12, 2, etc.). A script for creating these files automatically for any single or nested domain has been developed. This script, **create.FILES3**, can be run from the EDSS study planner and only requires two sets of user input (by way of environment variables). The required input are:

Table 6.3.1: Script variables in **create.FILES3**.

Environment Variable	Description	Example
EM_NEST_CT	Number of grid domains	5
EM_NEST_NO	Grid domain number definitions	"G0,G1,G2,G11,G12"

6.4 MEMORY SIZE DECLARATIONS

MAQSIP horizontal and vertical domain size declarations are defined in two include files: **HGRD_G*.EXT, VGRD_G*.EXT**. The "*****" signifies the number denoting a unique grid domain. A script for creating these files automatically for any single or nested domain has been developed. This script, **create.HVGRD3**, can be run from the EDSS

study planner and requires six sets of user input (by way of environment variables). The required input are:

Table 6.4.1: Script variables in **create.HVGRD3**.

Environment Variable	Description	Example
EM_NEST_CT	Number of grid domains	5
EM_NEST_NO	Grid domain number definitions	"G0,G1,G2,G11,G12"
EM_NCOLS	Number of columns in domains	"53,52,50,50,50"
EM_NROWS	Number of rows in domains	"53,49,50,50,50"
EM_NLAYS	Number of layers in domains	30
EM_NTHIK	Number of cells in boundaries	"1,1,1,1,1"

6.5 SPECIES LISTS

The full chemistry species declarations are defined in **SPCS3_XXXX.EXT**. Each transport process also has a species list. These lists are **ADV3_XXXX.EXT** for the advected species, **DIF3_XXXX.EXT** for the diffused species, **DDEP3_XXXX.EXT** for the deposited species, and **EMIS3_XXXX.EXT** for the emitted species. These files can be obtained from *sams* from the module *species*. The expression "**XXXX**" represents a substitution for the model that is being simulated by MAQSIP. Currently, there are two possibilities: **RADM** and **SAQM**. Eventually, all of these lists of chemistry species declarations will be produced by a generalized chemistry reader.

There do exist additional species lists for the simulated RADM model. MAQSIP allows for a mass adjustment (see Section 4.5.5) similar to the SAQM model. To allow build this model with MAQSIP, the **SPCS3_RADM_MADJ.EXT** and the **ADV3_RADM_MADJ.EXT** include files must be used. These include files can also be obtained from the *sams* module *species*..

6.6 CHEMISTRY PROCESSOR DECLARATIONS

The chemistry mechanism in MAQSIP requires three include files. The include file which defines the constants for the chemistry solver is **CHEMCONST_XXXX.EXT**. **MECHANISM_XXXX.EXT** contains the parameterization for the gas-phase chemical mechanism. The parameters used in interpolating photolytic rates in the gas-phase chemistry mechanism are defined in **PHOTLYTK_XXXX.EXT**. These files can be obtained from *sams* from the module *shared*.

6.7 CLOUD PROCESSOR DECLARATIONS

The cloud processor requires two include files: **CLDAQ3_XXXX.EXT** and **WDEP3_XXXX.EXT**. These files contain the species lists for cloud-aqueous chemistry and wet deposition, respectively. These files can be obtained from *sams* from the module *species*.

SECTION 7: REQUIRED INPUT

7.1 MODELS 3 I/O FILE NAMING CONVENTION

The Models 3 I/O structure provides a file naming convention. This convention produces filenames with four segments (each separated by an underscore) which fully describe the type of data each file contains. Therefore, all data can be placed/retrieved uniquely into/from a file. This reduces any uncertainty as to the location of placement of certain data and provides a simple means of naming any other needed files.

This EPS image does not contain a screen preview.

It will print correctly to a PostScript printer.

File Name : look.ps

Title : look.ps

Creator : XV Version 3.00 Rev: 3/30/93 - by John Bradley

Pages : 1

Figure 7.1.1 Data spatial locations

The first naming segment describes the time dependency general type of the data.

GRID   time independent data (only grid dependent)

MET   time dependent data (meteorology data)

CHEM   chemistry dependent data (species concentrations)

The second naming segment further describes the type of data contained in the file.

DOT   data is located at the dot locations (GRID, MET, CHEM)

CRO   data is located at the cross locations (GRID, MET, CHEM)

BDY   data is located at the boundary locations (GRID, MET, CHEM)

INIT   initial condition data (CHEM)

EMIS   emission data (CHEM)

CONC   output data (CHEM)

DRY   dry deposition data (CHEM)

WET   wet deposition data (CHEM)

KF   Kain-Fritsch cloud data by event (MET)

KFQA   gridded Kain-Fritsch cloud data for quality analysis (MET)

The third naming segment describes the dimensionality of the data.

1D   scalar data (MET)

2D   single-layered data (GRID, MET, CHEM)

3D   multi-layered data (GRID, MET, CHEM)

The last naming segment describes which domain (grid) the data belongs. Some examples of these segments are:

G0   coarse grid domain

G1   fine grid domain #1, contained in G0

G2   fine grid domain #2, contained in G0

G21   fine grid domain #1, contained in G2

Spatial data locations are illustrated in Figure 7.1.1. Each of these filenames are defined in the Models 3 include file *FILES3.EXT*.

7.2 INPUT DATA FOR EACH MODULE

This section contains lists of data needed for each module of MAQSIP. Some modules do not require any input and are shown here without any required data listed. For those modules that require input, the input variable name, units, description and file location are specified. The input files are currently produced by one of four different processors: MCIP (Meteorology Chemistry Interface Processor), SMOKE (Sparse Matrix Operator Kernel Emissions), Boundary Condition Processor, or Initial Condition Processor. The files beginning with "GRID" or "MET" are produced by MCIP. CHEM_EMIS_3D is produced by SMOKE. The files CHEM_INIT_3D and CHEM_BDY_3D are produced by the initial condition and boundary condition processors, respectively.

7.2.1 Driver Module

7.2.2 Convert Module

convert.F

DENS	$\frac{kg}{m^3}$	air density	MET_CRO_3D

inbdycon.F

DENS	$\frac{kg}{m^3}$	air density	MET_BDY_3D
BCON	*ppm*	boundary concentrations	CHEM_BDY_3D

7.2.3 Initialization Module

initscen.F

ICON	*ppm*	initial concentrations	CHEM_INIT_3D

7.2.4 Timestep Module

7.2.5 Advection Module

adj_con.F

DENS $\frac{kg}{m^3}$ air density MET_CRO_3D

7.2.6 Diffusion Module

hdiff.F

DENS	$\dfrac{kg}{m^3}$	air density	MET_CRO_3D
DENS	$\dfrac{kg}{m^3}$	air density	MET_BDY_3D

vdiff.F

DENS	$\dfrac{kg}{m^3}$	air density	MET_CRO_3D
VDEP	$\dfrac{m}{s}$	deposition velocity for deposited species	MET_CRO_2D
EMIS	$\dfrac{g}{s}$	emitted concentrations	CHEM_EMIS_3D

edyintb.F

UWIND	$\dfrac{m}{s}$	u component of horizontal wind	MET_DOT_3D
VWIND	$\dfrac{m}{s}$	v component of horizontal wind	MET_DOT_3D
PBL	m	planetary boundary layer height	MET_CRO_2D
USTAR	$\dfrac{m}{s}$	horizontal friction velocity	MET_CRO_2D
WSTAR	$\dfrac{m}{s}$	convective velocity scale	MET_CRO_2D
MOL	$\dfrac{1}{m}$	inverse Monin-Obukhov Length	MET_CRO_2D
TA	K	air temperature	MET_CRO_3D
QV	$\dfrac{g\ water}{g\ air}$	specific humidity	MET_CRO_3D
PRES	Pa	air pressure	MET_CRO_3D

7.2.7 Chemistry Module

gaschem.F

LAT	deg	latitude (south negative)	GRID_CRO_2D
LON	deg	longitude (west negative)	GRID_CRO_2D
MSFX2		squared map-scale factor (CROSS)	GRID_CRO_2D
HT	*m*	terrain elevation	GRID_CRO_2D
WBAR	$\frac{g}{m^3}$	average liquid water content of clouds	MET_CRO_2D
CLDB	*m*	cloud bottom	MET_CRO_2D
CLDT	*m*	cloud top	MET_CRO_2D
CFRAC		total fractional cloud coverage	MET_CRO_2D
TA	*K*	air temperature	MET_CRO_3D
QV	$\frac{g\ water}{g\ air}$	specific humidity	MET_CRO_3D
PRES	*Pa*	air pressure	MET_CRO_3D

7.2.8 Cloud Module

cldprocr.F

RN	*cm*	accumulated nonconvective precipitation	MET_CRO_2D
RC	*cm*	accumulated convective precipitation	MET_CRO_2D
TA	*K*	air temperature	MET_CRO_3D
QV	$\frac{g\ water}{g\ air}$	specific humidity	MET_CRO_3D
PRES	*Pa*	air pressure	MET_CRO_3D

7.2.9 Hydrostatic Sigma Pressure Coordinate Module

calcmet.F

MSFX2		squared map-scale factor (CROSS)	GRID_CRO_2D
MSFX2		squared map-scale factor (CROSS)	GRID_BDY_2D
PSTAR	*Pa*	pressure difference	MET_CRO_2D
PSTAR	*Pa*	pressure difference	MET_BDY_2D
DENS	$\frac{kg}{m^3}$	air density	MET_CRO_3D
DENS	$\frac{kg}{m^3}$	air density	MET_BDY_3D

height.F

ZH	m	mid-layer height above ground	MET_CRO_3D
ZF	m	full-layer height above ground	MET_CRO_3D

hcontvel.F

MSFD2		squared map-scale factor (DOT)	GRID_DOT_2D
UWIND	$\frac{m}{s}$	u component of horizontal wind	MET_DOT_3D
VWIND	$\frac{m}{s}$	v component of horizontal wind	MET_DOT_3D

vcontvel.F

MSFX2		squared map-scale factor (CROSS)	GRID_CRO_2D
MSFD2		squared map-scale factor (DOT)	GRID_DOT_2D
PSTAR	Pa	pressure difference	MET_CRO_2D
PSTAR	Pa	pressure difference	MET_BDY_2D

vcontdiff.F

PSTAR	Pa	pressure difference	MET_CRO_2D
DENS	$\frac{kg}{m^3}$	air density	MET_CRO_3D

depcontvel.F

PSTAR	Pa	pressure difference	MET_CRO_2D
DENS	$\frac{kg}{m^3}$	air density	MET_CRO_3D

7.2.10 Non-Hydrostatic Sigma-Pressure Coordinate Module

calcmet.F

PSTAR0	Pa	pressure difference	GRID_CRO_2D
PSTAR0	Pa	pressure difference	GRID_BDY_2D
DENS0	$\frac{kg}{m^3}$	reference density	GRID_CRO_3D
DENS0	$\frac{kg}{m^3}$	reference density	GRID_BDY_3D

height.F

ZH	m	mid-layer height above ground	GRID_CRO_3D
ZF	m	full-layer height above ground	GRID_CRO_3D

hcontvel.F

MSFD2		squared map-scale factor (DOT)	GRID_DOT_2D
UWIND	$\frac{m}{s}$	u component of horizontal wind	MET_DOT_3D
VWIND	$\frac{m}{s}$	v component of horizontal wind	MET_DOT_3D

vcontvel.F

PSTAR0	*Pa*	pressure difference	GRID_CRO_2D
PSTAR0	*Pa*	pressure difference	GRID_BDY_2D
DENS0	$\frac{kg}{m^3}$	reference density	GRID_CRO_3D
WWIND	$\frac{m}{s}$	vertical component of wind	MET_CRO_3D

vcontdiff.F

PSTAR0	*Pa*	pressure difference	GRID_CRO_2D
DENS0	$\frac{kg}{m^3}$	reference density	GRID_CRO_3D

depcontvel.F

PSTAR0	*Pa*	pressure difference	GRID_CRO_2D
DENS0	$\frac{kg}{m^3}$	reference density	GRID_CRO_3D

7.3 BOUNDARY INPUT DATA STRUCTURE

The files in Section 7.2 with the string "BDY" in their names contain boundary input data. This data has its own file structure. MAQSIP reads this data and correlates it with the interior data by the use of a pointer system. This pointer system designates the beginning location of the data in memory which starts a new side of the domain (e.g., South, East, North, and West). Figure 7.3.1 illustrates this input data structure and the relationship of the boundary data to the interior data within MAQSIP modules. Although the illustration contains a boundary thickness (NTHIK) of three cells, this method works for any boundary thickness.
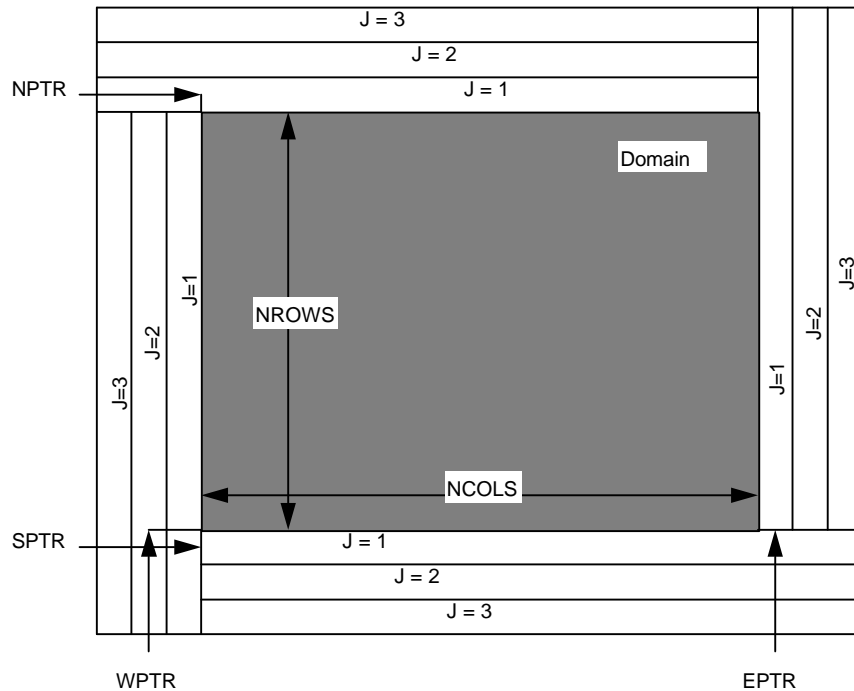
Figure 7.3.1   Boundary input data structure and relationship with the interior domain in MAQSIP.

The boundary data illustrated in Figure 7.3.1 is stored in a two dimensional array of size (2*(NCOLS + NROWS + 2*NTHIK), NTHIK). MAQSIP modules access this array using four pointers defined as:

South Pointer: SPTR = 0

East Pointer: EPTR = NCOLS + NTHIK

North Pointer: NPTR = NCOLS + NROWS + 3*NTHIK

West Pointer: WPTR = 2*NCOLS + NROWS + 4*NTHIK

These pointers are used in function statements so that data corresponding to each side of the domain can be accessed easily., For example, if the boundary data in Figure 7.3.1 is stored in array B, the function statements used to access the data corresponding to the four sides of the domain (South, East, North, and West) are:

S(COL, J) = B(SPTR + COL, J)

E(ROW, J) = B(EPTR + ROW, J)

N(COL, J) = B(NPTR + COL, J)

W(ROW, J) = B(WPTR + ROW, J)

The values of "COL" and "ROW" map directly with the values in the interior. The "J" value is the index of the boundary thickness (in Figure 7.3.1, J = 1, 2, or 3). Note that S, E, N, and W could not be defined as arrays that are EQUIVALENCEd to portions of B because they do not constitute contiguous portions of B.

SECTION 8: TEST CASES AND RESULTS

Test cases were generated for validing MAQSIP for the two coordinate systems currently implemented in Version 2.1: hydrostatic and non-hydrostatic sigma-pressure coordinates. Section 8.1 contains the test case descriptions and results for validating MAQSIP when sigma-pressure coordinates are used in hydrostatic mode. The results are compared with those from a previous version of the CTM. The latter model was previously validated by comparison to RADM. Section 8.2 contains the test case descriptions and results for validating MAQSIP when non-hydrostatic sigma-pressure coordinates are used in non-hydrostatic mode. Quantitative comparisons of MAQSIP with SAQM are presented for validation.

8.1 HYDROSTATIC SIGMA-PRESSURE COORDINATE TESTS

This section contains the test cases that are designed to validate MAQSIP for hydrostatic sigma-pressure coordinates. The main purpose for these tests is to phase out the previous CTM prototype that emulated RADM (referred here simply as the CTM). This requires MAQSIP to reproduce the results of the CTM (with the exception of those differences that are due to formulation changes made to the model). The CTM was previously validated by comparison to RADM for an August episode in 1988 over the Eastern United States and the results were published elsewhere (Odman et al., 1995; Byun et al, 1995). Here, MAQSIP is used to simulate the same episode and the results are compared to the CTM.

In this simulation, the domain is covered by 60x57 cells with 54-km grid size in the horizontal. There are 30 non-uniform vertical layers with increasing grid size (decreasing resolution) going from the surface to the top of the model. The meteorological data for the episode was derived from the hydrostatic Mesoscale Model (MM4). The RADM2 mechanism (Stockwell et al., 1990) is used to represent the chemical kinetics.

The appropriate input data to MAQSIP is generated using the same data used for the CTM simulations. The modifications to the original CTM data include changes to the units of pressure and density values, complience with MAQSIP's file naming convention, and moving some variables from one file to another according to MAQSIP's lists of variables in each file. Appendix C contains detailed information on the input data required by MAQSIP in hydrostatic mode.

Two comparison studies are performed: simulations using only the transport processes and simulations including the effects due to chemistry and clouds. The results from these two comparisons show the effects on the solution due to the model formulation changes. The formulation changes are as follows:

- the horizontal advection velocity for MAQSIP is the contravariant velocity (*Um*, *Vm*), while the CTM used U/m and V/m advection velocities and $\Delta x/m^2$ and $\Delta y/m^2$ grid spacing.

- the one dimensional transport processes is now ordered in an anti-biasing fashion.

First is the comparison of the CTM simulations with MAQSIP simulations using only the transport processes (i.e., advection and diffusion). Figure 8.1 illustrates the daytime averaged transported ozone values obtained from MAQSIP plotted against those obtained from the CTM for the first layer. Some statistical measures are given in Table 8.1 for comparison. The minor effects due to the change in advection velocity definitions and the anti-bias reordering of the one-dimensional transport processes are inherent in the results.

Second is the comparison of the CTM simulations with MAQSIP simulations including the effects due to chemistry and clouds. Figures 8.2 - 8.4 illustrate the daytime averaged values of NO, NO_2 and O_3 obtained from MAQSIP plotted versus those obtained from the CTM for the first layer. Statistical measure for comparisons are also provided in Tables 8.2 - 8.3. Notice, that the differences between the CTM and MAQSIP results are similar to those recorded in the transport simulations above, and that they are small even with the inclusion of chemistry and cloud effects. These results illustrate that MAQSIP and the CTM produce similar results for the hydrostatic sigma-pressure coordinates.

8.2 NON-HYDROSTATIC SIGMA-PRESSURE COORDINATE TESTS

This section contains the test cases that are designed to validate the results of MAQSIP for non-hydrostatic sigma-pressure coordinates. MAQSIP simulations are compared to simulations made by the SARMAP Air Quality Model (SAQM) for a two-day episode (2-3 August, 1990) in Central California. This episode was extensively studied using SAQM (CARB, 19xx). The modeling domain extends from San Francisco Bay to the Sierra Nevadas and covers most of the San Joaquin Valley . Both models use 32x39 cells in the horizontal (excluding the boundary cells) with a 12-km grid size. There are 15 vertical layers of non-uniform spacing between the surface and the top of the models. The vertical resolution is highest near the surface (first layer grid size is

approximately 60 m) and decreases (the grid size increases) towards the top. The CBM4 mechanism (Gery et al, 1989) extended by sulfur chemistry is used by both models.

The input data used by SAQM (meteorology, emissions, initial and boundary conditions) was obtained from California Air Resources Board and converted to the format required by MAQSIP. The original meteorological data was derived from the nonhydrostatic Mesoscale Model (MM5). Appendix C contains detail information on the input files required for MAQSIP in non-hydrostatic mode.
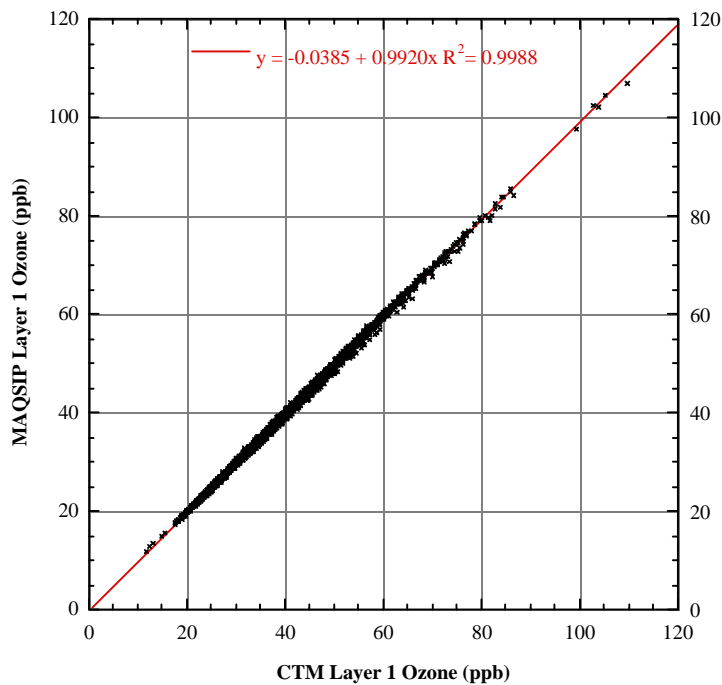
Figure 8.1.1 Transported ozone comparison for MAQSIP and the CTM.

Table 8.1.1 Comparison of transported O_3 estimates obtained from CTM and MAQSIP

	CTM O_3	MAQSIP O_3
Minimum	11.657	11.666
Maximum	109.60	106.82

|		
Sum	137475.16	136242.73
Points	3420	3420
Mean	40.20	39.84
Median	38.27	37.96
RMS	42.05	41.67
Std Deviation	12.33	12.24
Variance	152.04	149.80
Std Error	0.2108	0.2093
Skewness	0.8072	0.7953
Kurtosis	1.135	1.058
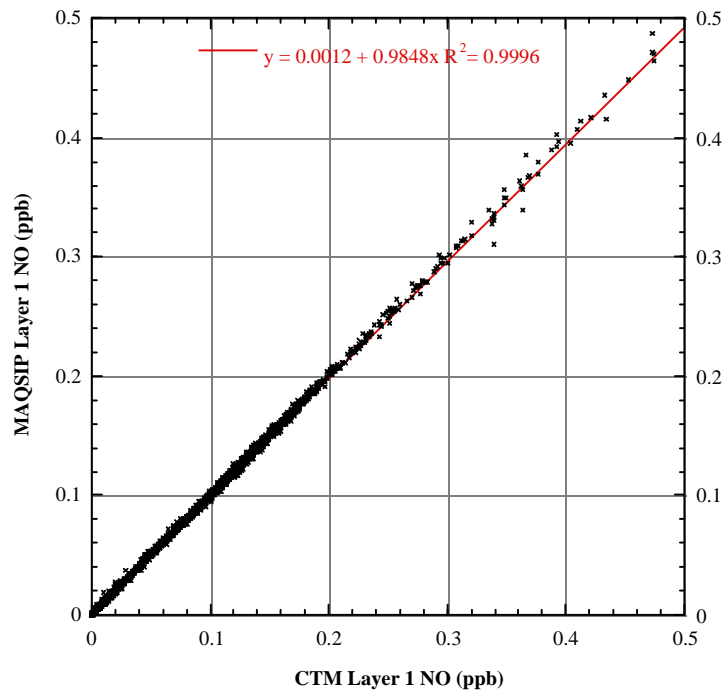
Figure 8.1.2 NO comparison for MAQSIP and the CTM.

Table 8.1.2 Comparison of NO estimates obtained from CTM and MAQSIP

	CTM NO	MAQSIP NO
Minimum	0.0001578	0.0001191
Maximum	7.661	7.447
Sum	250.65	250.95
Points	3420	3420
Mean	0.07329	0.07338
Median	0.03774	0.03813
RMS	0.1889	0.1865
Std Deviation	0.1741	0.1715
Variance	0.03030	0.02940
Std Error	0.002977	0.002932
Skewness	28.122	27.367
Kurtosis	1124.13	1073.74

$y = -0.0042 + 1.0062x \quad R^2 = 0.9998$

MAQSIP Layer 1 NO2 (ppb)

CTM Layer 1 NO2 (ppb)
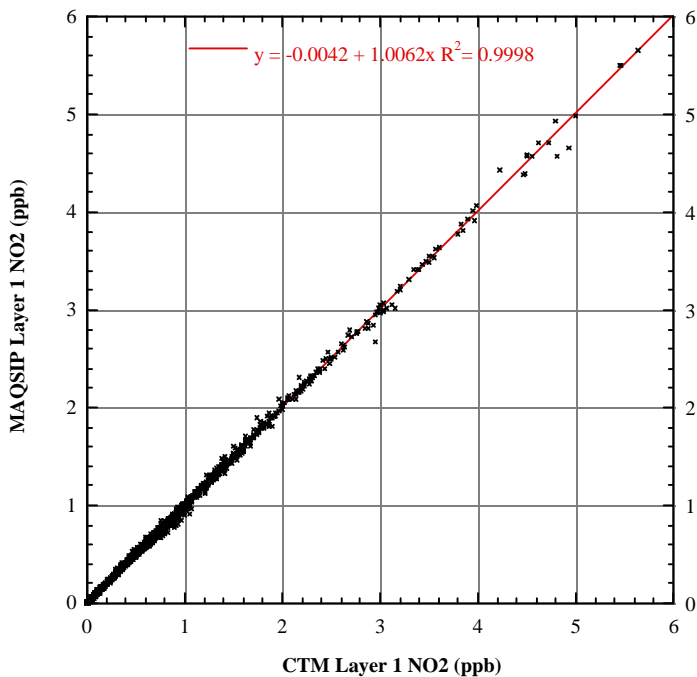
Figure 8.1.3 NO_2 comparison for MAQSIP and the CTM.

Table 8.1.3 Comparison of NO_2 estimates obtained from CTM and MAQSIP

	CTM NO_2	MAQSIP NO_2
Minimum	0.0005707	0.0004289
Maximum	50.46	51.04
Sum	1909.38	1906.87
Points	3420	3420
Mean	0.5583	0.5576
Median	0.2353	0.2336
RMS	1.5465	1.5548
Std Deviation	1.4425	1.4516
Variance	2.0807	2.1072
Std Error	0.02467	0.02482
Skewness	21.176	21.341
Kurtosis	640.21	648.31
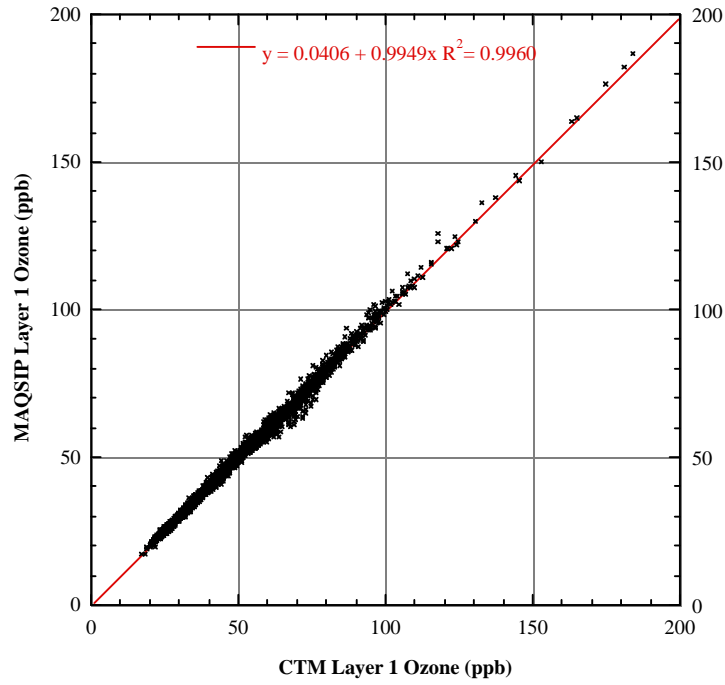
Figure 8.1.4 Ozone comparison for MAQSIP and the CTM.

Table 8.1.4. Comparison of O_3 estimates obtained from CTM and MAQSIP

	CTM O_3	MAQSIP O_3
Minimum	17.48	17.22
Maximum	184.21	187.10
Sum	167402.08	166686.65
Points	3420	3420
Mean	48.95	48.74
Median	45.35	45.37
RMS	52.86	52.64
Std Deviation	19.96	19.89
Variance	398.2	395.7
Std Error	0.3412	0.3402

Skewness	1.223	1.282
Kurtosis	2.862	3.147

Three tests cases are presented here where both models are configured with the following processes: 1) Horizontal advection only, 2) Transport (advection and turbulent diffusion) only, and 3) Chemistry and transport (i.e., all model processes with the exception of clouds).

8.2.1 Horizontal Advection Test

Starting at 12:00 GMT on 2 August 1990, the initial concentrations are advected horizontally for 48 hrs using the MM5-derived wind fields. For this test, the MAQSIP code is modified to match the SAQM code. These modifications include: 1) Using a fixed time step of 2.5 min, 2) Using the same boundary conditions as in SAQM, 3) Advecting cp_0^*/ρ_0 with U/m and using a grid size of $\Delta x/m^2$, and 4) Using molecules $/cm^3$ units for c.

Scatter plots of the results (MAQSIP vs SAQM) for O_3 and NO_2 are shown in Figures 8.2.1 and 8.2.2 and the statistics are summarized in Tables 8.2.1 and 8.2.2. The displayed results are average concentrations for the first layer (the layer closest to the surface) cells where there are reporting observation stations (126 stations for O_3 and 75 stations for NO_2). Initial values and the estimates for all 48 hours of the simulation are displayed. It should be noticed that there are more than one station in some cells, therefore the same cell averaged concentration may have been counted more then once. Also, since the initial values are the same, the differences may be slighly reduced.

Both O_3 and NO_2 estimates derived from MAQSIP and SAQM are virtually identical. Note that the initial distribution of O3 and NO_2 are highly non-uniform and they are very different from each other. Advecting highly non-uniform distributions would stress the differences between the horizontal advection processes of the two models, if there were any. However, no significant differences are observed. Also, the models produce very similar resuls for two species with very different distributions, suggesting that the horizontal advection is treated in the same manner by both models. Thus, MAQSIP can emulate the horizontal advection process in SAQM almost exactly if the modifications listed above are performed. However, since there are disadvantages to the choices made in SAQM, MAQSIP will be used without these modifications from here on.

8.2.2 Transport Test

In this test, the initial concentrations are transported for 48 hrs using the MM5-derived wind and mixing fields, starting at 12:00 GMT on 2 August 1990. Recall that the transport processes of MAQSIP consist of horizontal and vertical advection and horizontal and vertical turbulent diffusion. SAQM includes the same transport processes, however, there are some important differences between the formulations of MAQSIP and SAQM. These are:
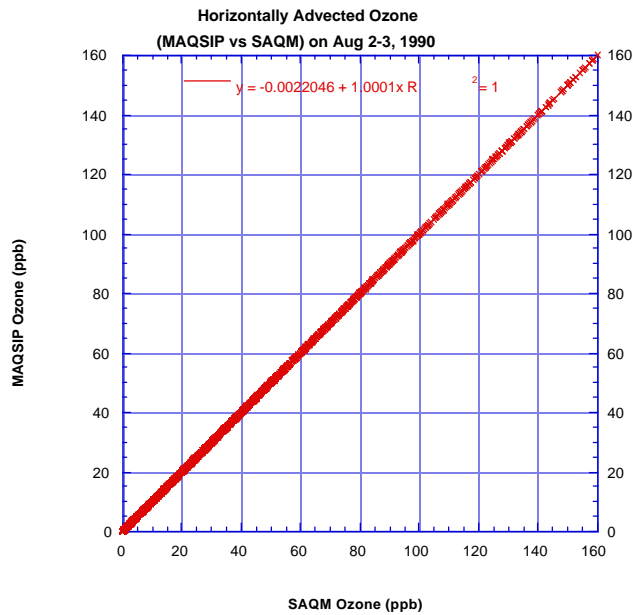
Horizontally Advected Ozone
(MAQSIP vs SAQM) on Aug 2-3, 1990

$y = -0.0022046 + 1.0001x \quad R^2 = 1$
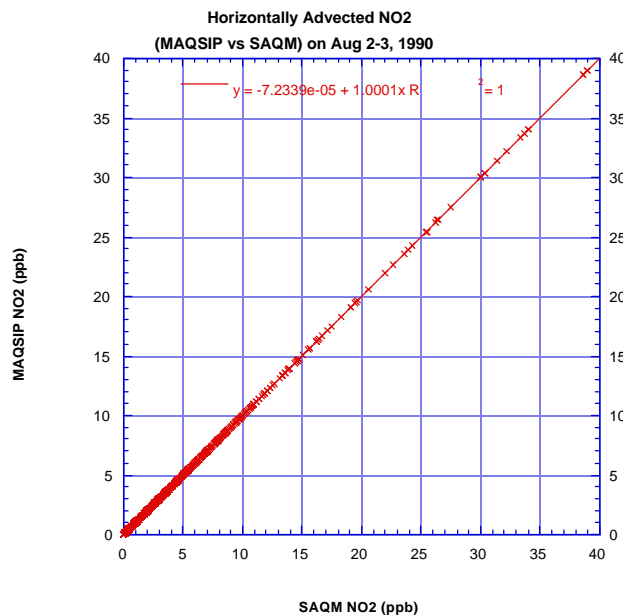
MAQSIP Ozone (ppb)

SAQM Ozone (ppb)

Figure 8.2.1 Correlation of horizontally advected O_3 (MAQSIP vs SAQM) at 126 surface sites for 49 hrs (Starting at 12:00 GMT on 2 August 1990).

Table 8.2.1 Comparison of horizontally advected O_3 estimates obtained from SAQM and MAQSIP

	SAQM O_3	MAQSIP O_3
Minimum	0	0
Maximum	706.67	706.98
Sum	220912.66	220916.64

Points	6174	6174
Mean	35.78	35.78
Median	19.695	19.685
RMS	67.208	67.212
Std Deviation	56.896	56.900
Variance	3237.13	3237.65
Std Error	0.724	0.724
Skewness	4.313	4.313
Kurtosis	27.57	27.58

Horizontally Advected NO2
(MAQSIP vs SAQM) on Aug 2-3, 1990

$y = -7.2339e\text{-}05 + 1.0001x \quad R^2 = 1$

MAQSIP NO2 (ppb)

SAQM NO2 (ppb)

Figure 8.2.2 Correlation of horizontally advected NO_2 (MAQSIP vs SAQM) at 75
surface sites for 49 hrs (Starting at 12:00 GMT on 2 August 1990).

Table 8.2.2 Comparison of horizontally advected NO_2 estimates obtained from
SAQM and MAQSIP

	SAQM NO_2	MAQSIP NO_2

Minimum	0	0
Maximum	38.96	38.96
Sum	7380.84	7380.98
Points	3675	3675
Mean	2.008	2.008
Median	0.670	0.670
RMS	4.160	4.160
Std Deviation	3.644	3.644
Variance	13.278	13.279
Std Error	0.0601	0.0601
Skewness	4.529	4.529
Kurtosis	30.151	30.149

1) The boundary conditions: SAQM uses a zeroth order polynomial to compute the advective flux coming into the domain, i.e., $F_{in} = u_{1/2}c_0$ or $u_{N+1/2}c_{N+1}$, while MAQSIP uses a first order polynomial. The outflow boundary condition sets the concentration gradient to zero, i.e., $c_0 = c_1$ or $c_{N+1} = c_N$, while MAQSIP uses a no flux-gradient condition.

2) SAQM uses a fixed time step of 2.5 min while MAQSIP may select a different time step every hour depending on the wind velocities. In this simulation, there are several instances when the Courant stability limit is exceeded with the 2.5 min time step during vertical advection. MAQSIP time steps range from 1 min to 5 min.

3) In the horizontal, SAQM advects the scalar quantity cp_0^* / ρ_0 with a velocity equal to U / m or V / m and uses a grid spacing of $\Delta x / m^2$ or $\Delta y / m^2$. The spatial variation of grid spacing is not accounted for in the advection solver. MAQSIP, on the other hand, advects $cp_0^* / m^2 \rho_0$ with the contravariant velocity Um or Vm and uses a uniform grid spacing of Δx or Δy.

4) The units of c in SAQM are $molecules / cm^3$, thus the value of c is large. The units used in MAQSIP are $\mu g / m^3$. For this reason, SAQM is more prone to round-off errors on some computers than MAQSIP. However, the effect of this difference is marginal on 64-bit machines.

5) The parameterization of vertical diffusion is different between the two models. MAQSIP uses the classical K-theory while SAQM uses asymmetric mixing coefficients (top-down mixing is different than bottom-up) as described in (Pleim and Chang, 1992).

6) Some quantities are different in the two models. For example, in MAQSIP, air densities are computed from hourly pressure and temperatures, stored as hourly data, and then interpolated in time. On the other hand, in SAQM, pressures and temperatures are interpolated in time and the densities are computed from these interpolated values. However, such differences have usually a marginal effect on model predictions.

7) Most meteorological variables are interpolated to the middle of the time step in MAQSIP while they are interpolated to the beginning of the time step in SAQM.

A scatter plot of the transported O_3 estimates (MAQSIP vs SAQM) are shown in Figures 8.2.3 and the statistics are summarized in Tables 8.2.3. Once again the displayed results are average concentrations for the first layer cells where there are reporting observation stations (126 stations report O_3 during this 48-hour simulation). The estimates of O_3 derived from MAQSIP are somewhat different from SAQM estimates, as evidenced in Figure 8.2.3. Also, some metrics such as the minimum, variance, skewness andkurtosis are different. However, these differences can be explained by the formulation differences stated above. The formulation difference that has the largest effect on the transported O_3 estimates is the parameterization of vertical diffusion. Note that results for
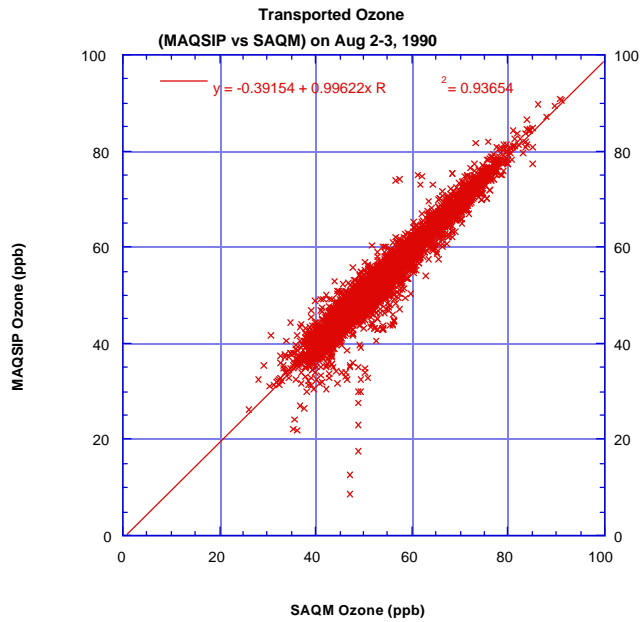
Figure 8.2.3 Correlation of transported O_3 (MAQSIP vs SAQM) at 126 surface sites for 49 hrs (Starting at 12:00 GMT on 2 August 1990).

Table 8.2.3 Comparison of transported O_3 estimates obtained from SAQM and MAQSIP

	SAQM O_3	MAQSIP O_3
Minimum	26.14	8.61
Maximum	91.24	90.94
Sum	335020.94	331336.07
Points	6174	6174
Mean	54.26	53.67
Median	52.82	52.30
RMS	55.07	54.53
Std Deviation	9.391	9.667
Variance	88.19	93.45
Std Error	0.1195	0.1230

Skewness	0.5927	0.4992
Kurtosis	0.1333	0.2846

NO_2 could not be compared because MAQSIP injects emissions in the vertical diffusion process while SAQM does so in chemistry. Thus, only non-emitted species could be compared in this transport test.

8.2.3 Transport and Chemistry Test

In this test, all the transport and chemistry processes of the two models are active with the exception of cloud processes. The 48-hour simulation starts at 12:00 Z (4:00 PST) on 2 August 1990. In addition to the transport differences mentioned in Section 8.2.2, first there are differences between the chemistry solvers of the two models. Second, MAQSIP injects the emissions during the horizontal diffusion process while SAQM does this in the gas-phase chemistry module. This may have some effect on the short-lived species estimates.

There are 126 surface sites where observations of ozone are available during this episode. Figure 8.2.4 shows the domain and the locations of the observation sites. In Figure 8.2.5, ozone concentrations estimated by MAQSIP are compared to observations and those estimated by SAQM at the observation sites. In Figure 8.2.6, the cumulative distribution function and other statistics for the model estimates as well as observations are shown. In addition, various statistical measures for the observed and estimated O_3 concentrations are displayed in Table 8.2.4. Both models significantly overestimeate ozone concentrations. While more than 50% of all observations are below 40 ppb (the median is 30 ppb), the models have less than 10% of their predictions in this range. There is better agreement between observations and predictions for higher ozone concentrations. In general, MAQSIP's ozone estimates are lower than SAQM's. The median of ozone concentrations estimated by MAQSIP is 62 ppb compared to 64 ppb in SAQM. Also, the count of MAQSIP's predictions is higher in the 20-60 ppb range than SAQM's. However, the differences between the two models are small and they yield very similar ozone estimates as evidenced by an R2 of 0.96 in Figure 8.2.5-b and almost indistinguishable cumulative distribution functions up to the 99th percentile in Figure 8.2.6-a. Also, there is a remarkable similarity between the scatter plots of Figures 8.2.3 (transported ozone) and 8.2.6-b. This resemblance suggests that most of the differences between MAQSIP's and SAQM's ozone estimates are due to the differences in transport formulation (primarily the parameterization of vertical diffusion).

The spatial distribution of ozone is also very similar between the models. In Figure 8.2.7a, ozone concentrations as predicted by MAQSIP for 00:00 Z (16:00 PST) 4 August 1990 are shown as well as the observations. The model overestimates ozone in the Bay area (e.g., San Fransisco, Oakland), north and northwest of San Francisco Bay (e.g., Napa, Sonoma, and Santa Rosa) and along the coastline. This is primarily due to the inadequacy of boundary data along inflow boundaries and the inability of the model toproperly resolve urban NO_x plumes. There is better agreement between model predictions and observations in downwind regions and most of the San Joaquin Valley (e.g., Sacramento, Fresno, Bakersfield). The differences between MAQSIP and SAQM

This EPS image does not contain a screen preview.
It will print correctly to a PostScript printer.
File Name : Figure8.2.4.ps
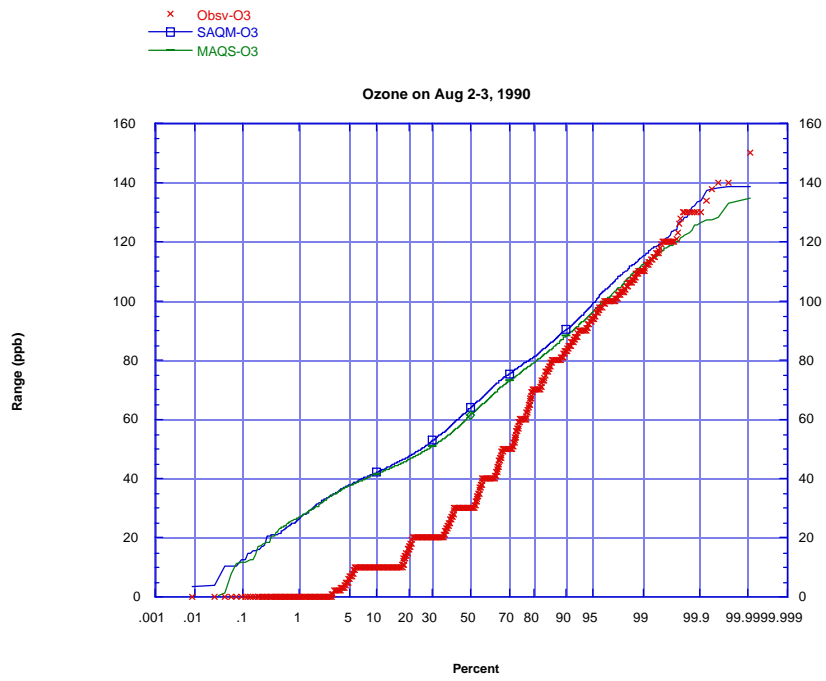
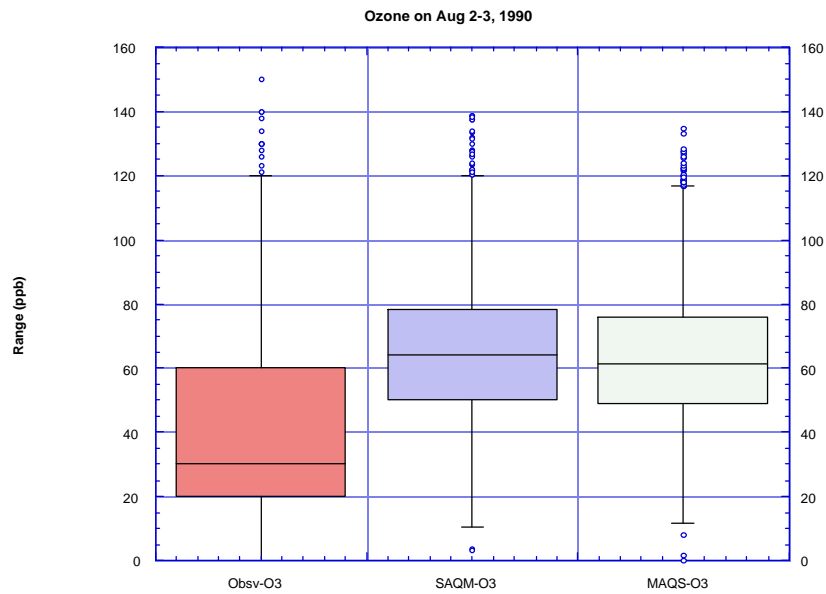Figure 8.2.4 Simulation domain and the locations of observation sites.
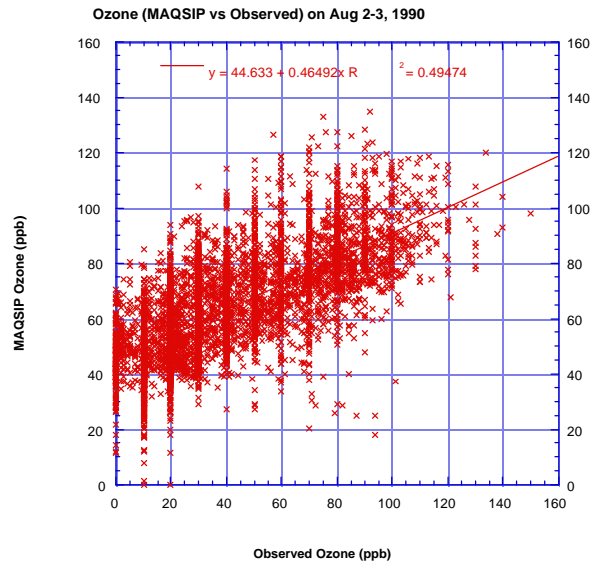
(a)
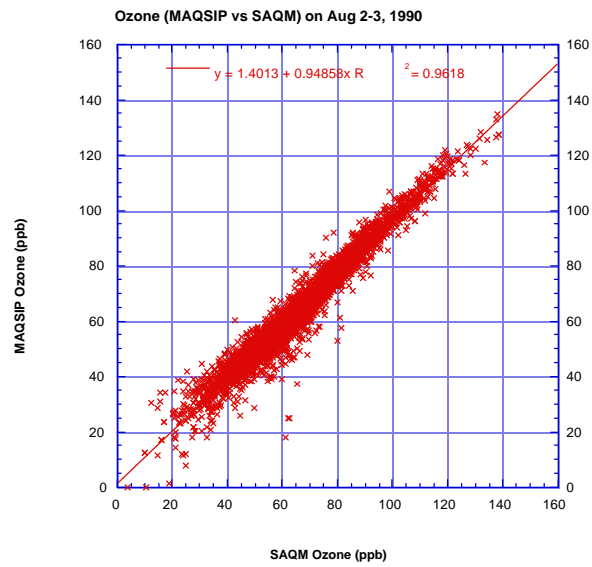
(b)

Figure 8.2.5 Correlation of O_3 at 126 surface sites: a) MAQSIP estimates versus observations, b) MAQSIP vs SAQM

(a)

(b)

Figure 8.2.6 Comparison of ozone estimates (MAQSIP and SAQM) and observations:
a) Cumulative distribution functions, b) Summary of the distributions

are shown in Figure 8.2.7b. While the differences are small after 36 hrs of simulation, there is considerable spatial variation that can be related to the differences in model formulations and particularly to the differences in the parameterization of vertical diffusion and those in chemistry solvers. The differences near the western and eastern boundaries are primarily due to the difference in the inflow and outflow boundary conditions of the two models. The difference over San Francisco Bay and the coastline may be due to the difference in the parameterization of vertical mixing. In Figure 8.2.8, the time variation of O_3 levels is shown at four sites. Again, MAQSIP estimates are almost identical to SAQM's. Both models overestimate ozone at Livermore and during the night at the other three sites.

There are 75 surface sites reporting NO_x observations for this simulations. In Figure 8.2.9, MAQSIP's estimates of NO_2 and NO are compared to those of SAQM at the observation sites. In Figures 8.2.10 and 8.2.11 cumulative distribution functions and other statistics about the distribution of the observations and model estimates are given for NO_2 and NO, respectively. In addition, various statistical measures for the observed and estimated NO_2 and NO concentrations are displayed in Tables 8.2.5 and 8.2.6. Both models significantly underestimate NO_x concentrations. In general, MAQSIP produces higher NO_x levels than SAQM but the differences are not very large (R2 is 0.91 for NO_2 and 0.82 for NO). The differences between model estimates are primarily due to the differences in the parameterization of vertical diffusion and in the chemistry solvers.

In summary, MAQSIP's performance in estimating ozone and related pollutant levels in the San Joaquin Valley is comparable to SAQM for the 2-3 August 1990 episode. This concludes the source code validation for the non-hydrostatic sigma-pressure coordinates.

Table 8.2.4 Comparison of O_3 observations and model estimates

	Observed O_3	SAQM O_3	MAQSIP O_3
Minimum	0.00	3.40	0.09
Maximum	150.00	138.63	134.67
Sum	231129.00	376207.31	364942.04
Points	5770.00	5770.00	5770.00
Mean	40.06	65.20	63.26
Median	30.00	64.02	61.54
RMS	49.05	68.01	65.97

|			
Std Deviation	28.30	19.36	18.71
Variance	801.08	374.70	349.99
Std Error	0.37	0.25	0.25
Skewness	0.77	0.38	0.43
Kurtosis	-0.26	0.03	-0.01

This EPS image does not contain a screen preview.
It will print correctly to a PostScript printer.
File Name : Figure8.2.7a.ps

Figure 8.2.7-a   MAQSIP estimates and observations of ozone levels on 00:00 Z
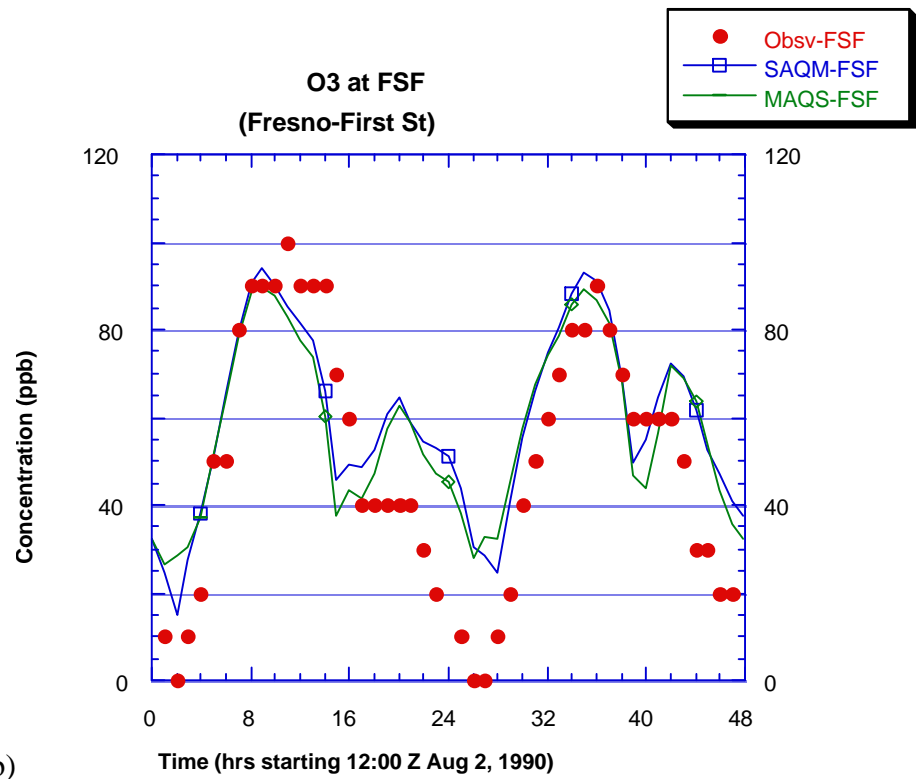(16:00 PST) 4 August 1990

This EPS image does not contain a screen preview.
It will print correctly to a PostScript printer.
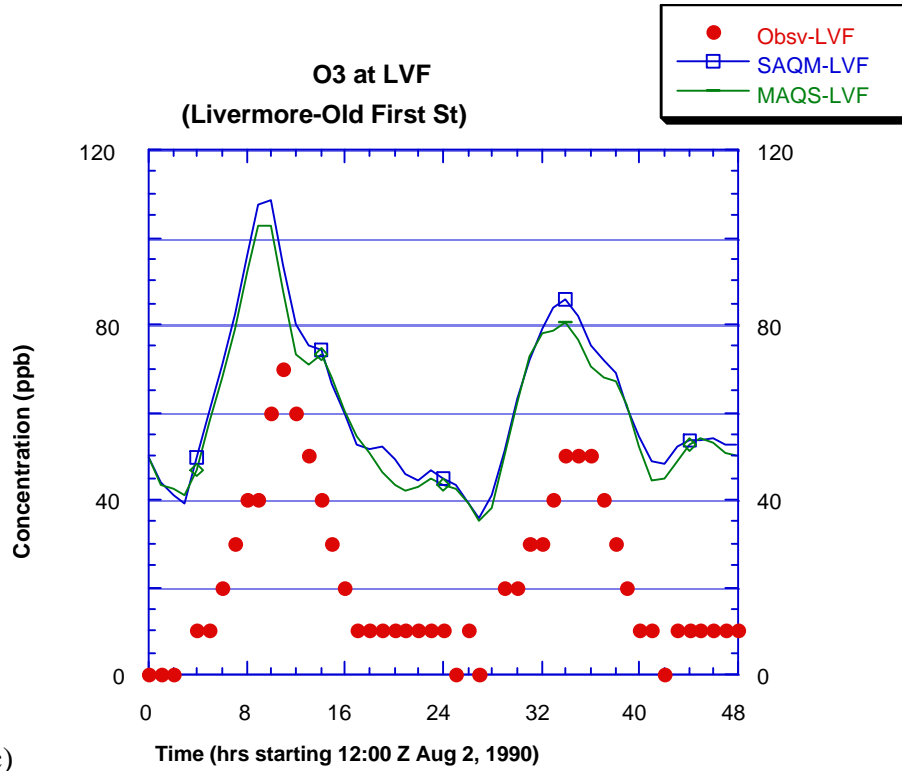File Name : Figure8.2.7b.ps

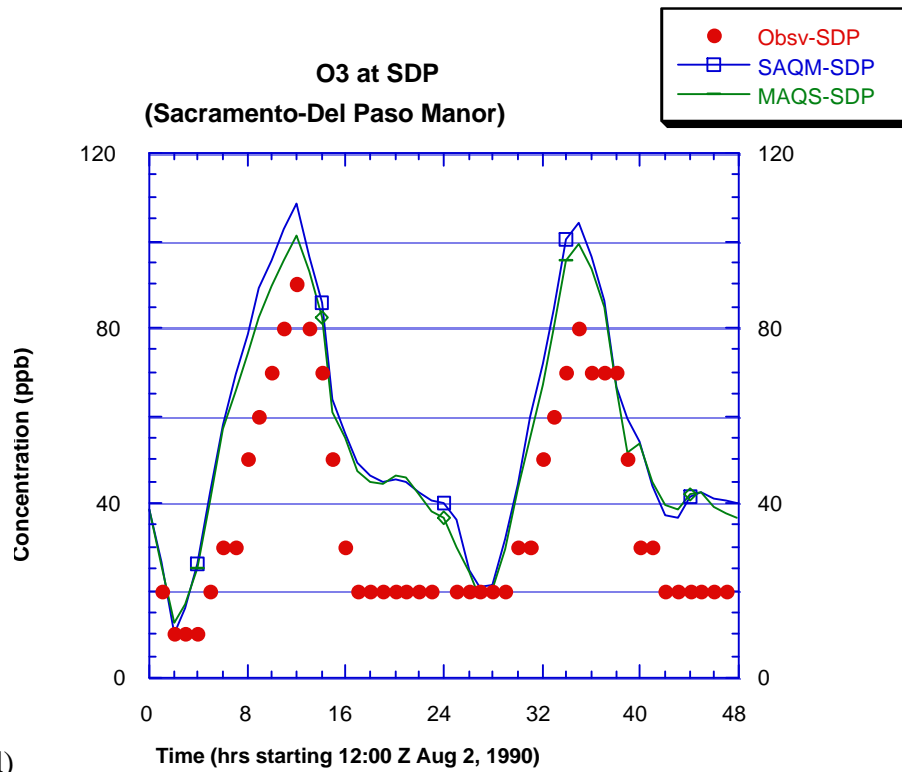Figure 8.2.7-b   Difference of MAQSIP and SAQM ozone levels on 00:00 Z (16:00 PST) 4 August 1990.
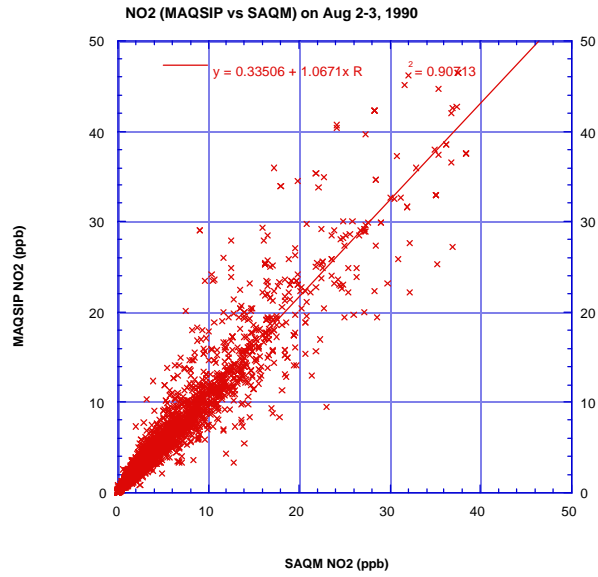
(a)

(b)

(c)

(d)
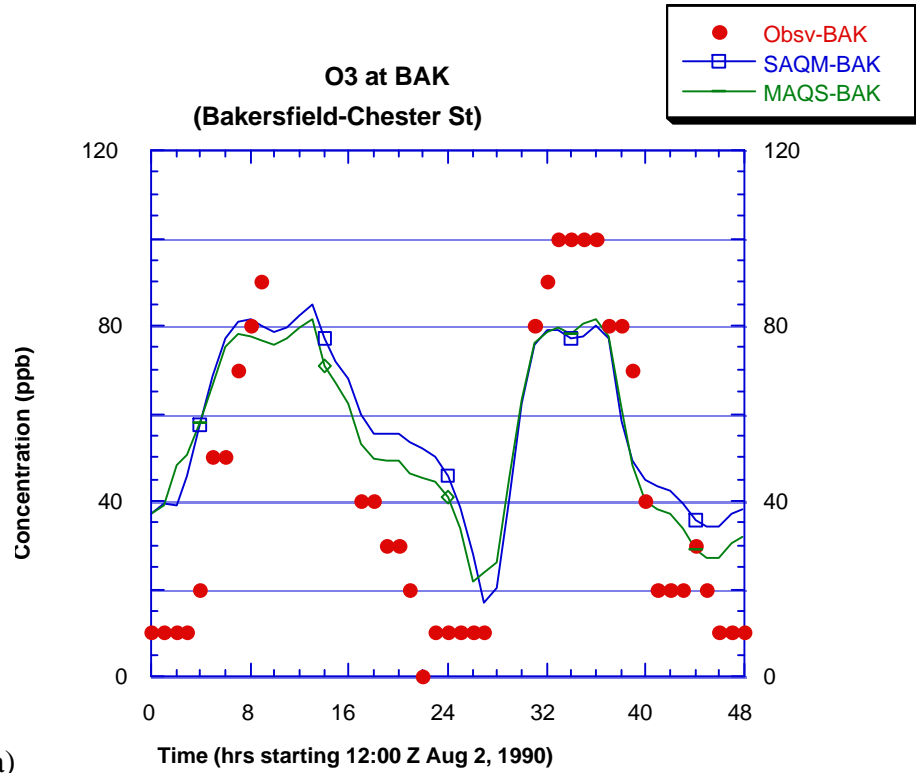
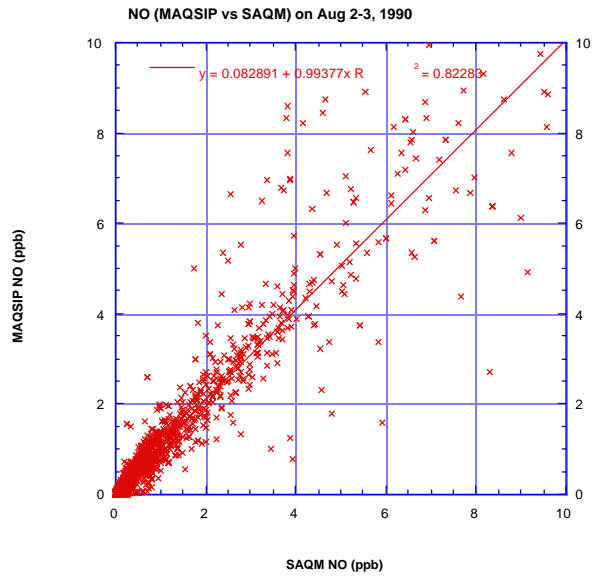Figure 8.2.8 Ozone time series at four sites: a) Bakersfield, b) Fresno, c) Livermore, and d) Sacramento.

NO2 (MAQSIP vs SAQM) on Aug 2-3, 1990

y = 0.33506 + 1.0671x R x^2 = 0.90713

MAQSIP NO2 (ppb)

SAQM NO2 (ppb)

(a)

NO (MAQSIP vs SAQM) on Aug 2-3, 1990

$y = 0.082891 + 0.99377x$ $R^2 = 0.82283$

(b)

Figure 8.2.9 Correlation of NO_x (MAQSIP vs SAQM) at 75 surface sites: a) NO_2 and
b) NO.

× Obsv-NO2
SAQM-NO2
MAQS-NO2

NO2 on Aug 2-3, 1990
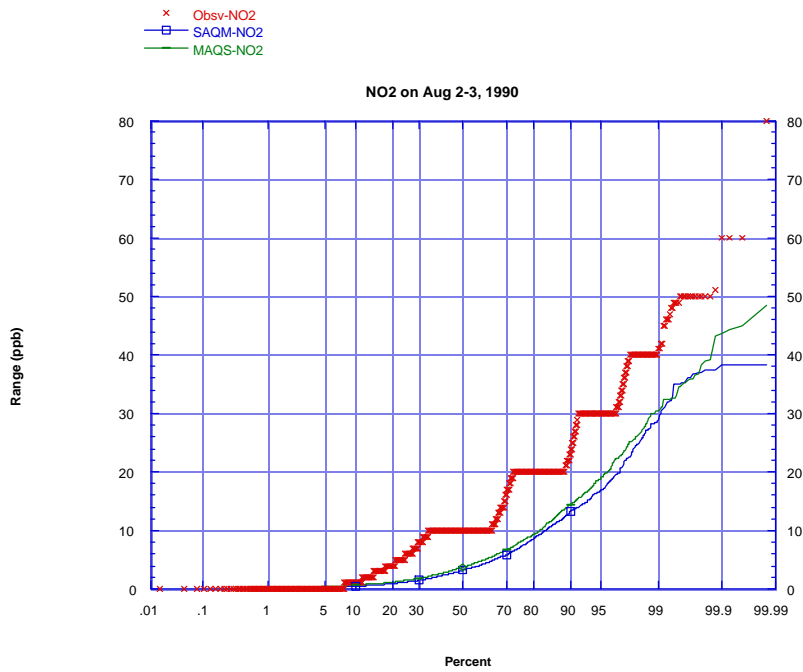
(a)
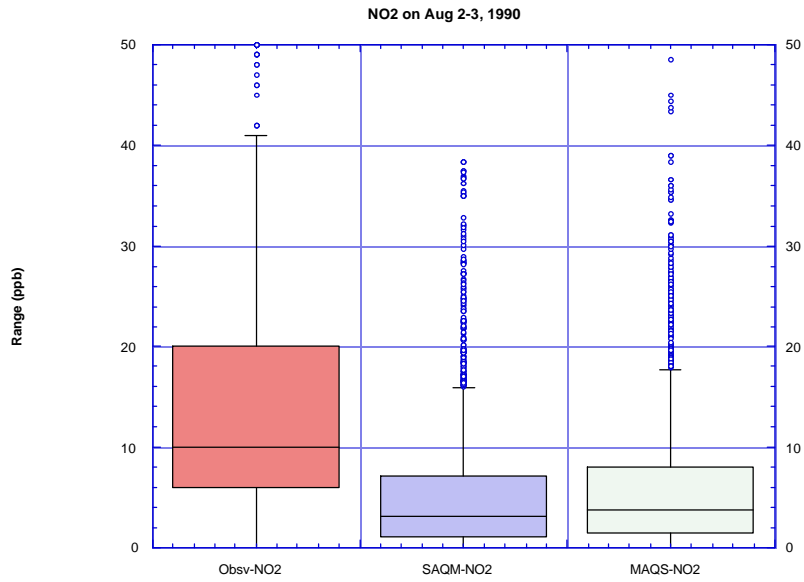
(b)

Figure 8.2.10 Comparison of NO₂ estimates (MAQSIP and SAQM) and
observations: a) Cumulative distribution functions, b) Summary of the
distributions.
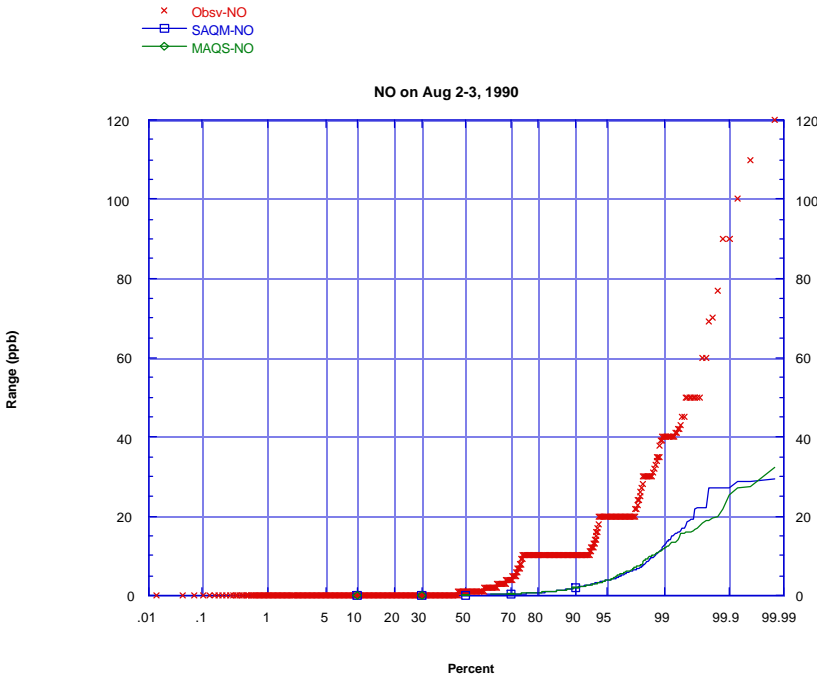
(a)
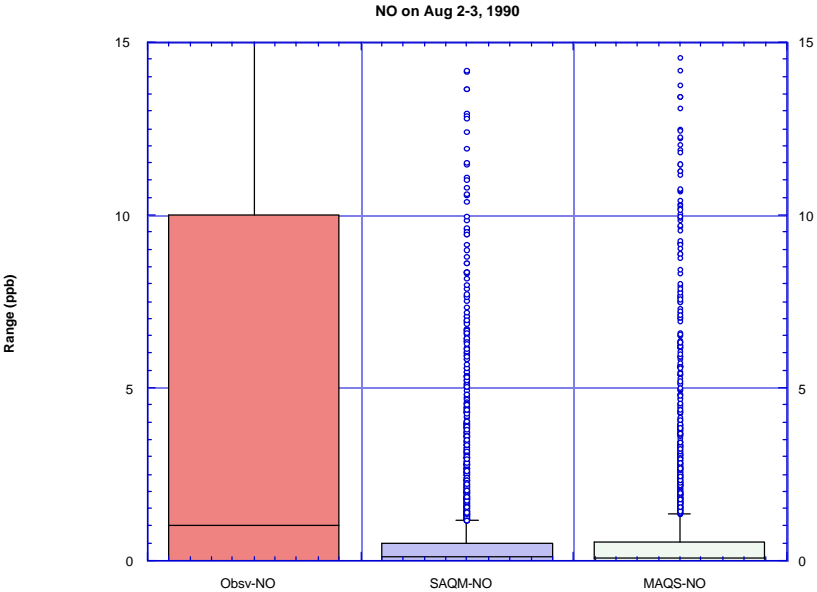

(b)

Figure 8.2.11   Comparison of NO estimates (MAQSIP and SAQM) and observations:
a) Cumulative distribution functions, b) Summary of the distributions.

Table 8.2.5 Comparison of NO_2 observations and model estimates

	Observed NO_2	SAQM NO_2	MAQSIP NO_2
Minimum	0.00	0.00	0.02
Maximum	80.00	38.36	48.45
Sum	41512.00	17832.14	19975.60
Points	3376.00	3376.00	3376.00
Mean	12.30	5.28	5.92
Median	10.00	3.18	3.74
RMS	15.57	8.00	8.74
Std Deviation	9.55	6.02	6.43
Variance	91.13	36.19	41.35
Std Error	0.16	0.10	0.11
Skewness	1.27	2.20	2.11
Kurtosis	2.47	6.18	5.63

Table 8.2.6 Comparison of NO observations and model estimates

	Observed NO	SAQM NO	MAQSIP NO
Minimum	0.00	0.00	0.00
Maximum	120.00	29.28	32.41
Sum	14983.00	2747.82	2688.21
Points	3400.00	3400.00	3400.00
Mean	4.41	0.81	0.79
Median	1.00	0.11	0.08
RMS	9.32	2.55	2.38
Std Deviation	8.21	2.42	2.25
Variance	67.40	5.85	5.05
Std Error	0.14	0.04	0.04
Skewness	4.80	6.62	5.97
Kurtosis	40.71	55.72	47.73

SECTION 9: SUMMARY AND CONCLUSIONS

MAQSIP is a state-of-the-art air quality modeling platform developed at MCNC–North Carolina Supercomputing Center. This report documents the source code for basic modules of MAQSIP used for ozone air quality modeling. It also describes the input parameter and data requirements for typical ozone air quality simulations.

MAQSIP is developed in a truly modular fashion where modules for different processes (e.g., advection, diffusion, chemistry) operate on a common pollutant concentration array. MAQSIP provides alternative modules for various processes allowing the user to select his/her favorite process representation or solution algorithm. For example, two chemistry mechanisms are supported: RADM2 and CBM4. MAQSIP is formulated in such a way that any coordinate system can be used. This document emphasizes the generalized-coordinate feature and discusses in detail the two coordinate systems implemented in Version 2.1. These are the hydrostatic sigma-pressure and non-hydrostatic sigma-pressure (equivalent to sigma-altitude) coordinates. Implicit in these coordinate systems are the two modes of operation for MAQSIP: one that assumes a hydrostatic atmosphere and the other that does not. In non-hydrostatic mode, MAQSIP conforms better with meteorological data coming from non-hydrostatic mesoscale models (e.g., MM5). The modules of MAQSIP are classified as coordinate dependent and coordinate independent. Version 2.1 contains coordinate dependent modules only for the two coordinate system mentioned above. However, this report and Srivastava et al (1994) contain enough detail for a user to create coordinate dependent modules for other coordinate systems.

Another purpose of this report was to validate MAQSIP, i.e., show that it can indeed be used for modeling ozone air quality. This is done for both modes of operation. For the hydrostatic mode, MAQSIP is tested against an earlier prototypical version (CTM). The latter was evaluated and also compared to RADM for an August, 1988 episode over the Eastern United States (Odman et al., 1995). MAQSIP produces similar results to those of the CTM. The differences are within the expected range, given the differences in model formulations. For the non-hydrostatic mode, MAQSIP was evaluated in an application to Central California and also compared to SAQM. It has been found that MAQSIP overestimates ozone for the 2-3 August 1990 period and significantly underestimates NOx. However, the estimates for ozone and related pollutants are similar to those of

SAQM. The differences between the two models can be related to the differences in the parameterization of vertical diffusion and chemistry solvers.

Version 2.1 of MAQSIP described in this document was released on 7 May 1996.

SECTION 10: REFERENCES

Anderson D.A., J.C. Tannehill, and R.H. Pletcher (1984). Computational Fluid Mechanics and Heat Transfer, McGraw-Hill, New York.

Ambrosiano, J., R. Balay, C. Coats, A. Eyth, S. Fine, D. Hils, T. Smith, S. Thorpe, T. Turner, and M. Vouk. The environmental decision support system: Air quality modeling and beyond. Proceedings of U.S. EPA Workshop on Next Generation Environmental Models Computational Methods, Bay City, MI, August 7-9, 1995, SIAM Publishers.

Bott, A. (1989a), "A positive definite advection scheme obtained by nonlinear renormalization of the advective fluxes," *Mon. Wea. Rev.* **117**, 1006-1015.

Bott, A. (1989b), "Reply," *Mon. Wea. Rev.* **117**, 2633-2636.

Byun, D.W., D. Dabdub, S. Fine, A. Hanna, R. Mathur, M.T. Odman, A.G. Russell, E.J. Segall, J.H. Seinfeld, P. Steenkiste, and J. Young. Emerging air quality modeling technologies for high performance computing and communication environments. Proceedings of the 21st NATO/CCMS International Technical Meeting on Air Pollution Modeling and its Application, Baltimore, MD, November 6-10, 1995.

CARB, 1996: Performance Evaluation of SAQM in Central California and Attainment Demonstration for the August 3-6, 1990 Ozone Episode. J. DaMassa, S. Tanrikulu, K. Magliano, A.J. Ranzieri, and L. Niccum.

Chang, J.S., R.A. Brost, I.S.A Isaksen, S. Madronich, P. Middleton, W.R. Stockwell, and C.J. Walcek (1987). "A Three - Dimensional Eulerian Acid Deposition Model: Physical Concepts and Formulation," *Journal of Geophysical Research* **Vol 92**, 14681-14700.

Gery, M.W., et al., 1989: A photochemical kinetics mechanism for urban and regional scale computer modeling. J. Geophys. Res., 94, 12,925-12,956.

Holton, J.R. (1992). An Introduction to Dynamic Meteorology. Academic Press Inc., New York.

Jin, S. and J.S. Chang (1993) : The SARMAP air quality model (SAQM), Presented at the A&WMA Specialty Conference, Regional Photochemical Measurement and Modeling Studies, San Diego, CA, November, 1993.

Odman, M.T., R. Mathur, K. Alapaty, R.K. Srivastava, D.S. McRae, and R.J.Yamartino. Nested and adaptive grids for multiscale air quality modeling. Proceedings of U.S. EPA Workshop on Next Generation Environmental Models Computational Methods, Bay City, MI, August 7-9, 1995, SIAM Publishers.

Pielke, R.A. (1984) Mesoscale Meteorological Modeling, Academic Press, New York, N.Y., 612 pg.

Pleim, J.E. and J.S. Chang (1992), "A non-local closure model for vertical mixing in the *Atmos. Environ.*, **26A**, 965-981.

Srivastava, R.K., McRae, D.S. and Odman, M.T. (1995), "Governing Equations of Atmospheric Diffusion," Technical Report, MCNC—North Carolina Supercomputing Center, Research Triangle Park, NC.

Stockwell, W.R., P. Middleton, and J.S. Chang, 1990: The second generation regional acid deposition model chemical mechanism for regional air quality modeling. J. Geophys. Res., 95, 16,343–16,367.

SECTION 11: APPENDIX A

11.1 CHARACTERISTICS OF MAQSIP

11.1.1 General Attributes

Input Requirements   Number of files required for each grid[#] per run

Emission file: 1

Initial conditions: 1

Boundary conditions: 1

Meteorology files: 5

Domain definition files: 5

Computer Platforms   Simulation: Current applications run on Cray YMP, C90, T90

Analysis and Preprocessing: DEC, SGI, SUN workstations

Hardware Requirements   Memory: 16Mwrds[*]

Input files: 335 Mbytes/day[*]

Output: 550 Mbytes/day[*]

CPU Time: 2 hr/day[*][†]

Software Requirements   UNIX, UNICOS, FORTRAN 77, C

Met Processing and Analysis: NCAR Graphics, IMSL

Emissions: SAS, ARC/INFO

Analysis: NCAR Graphics, AVS

Special Features   <u>Seasonal Simulation:</u> The capability to simulate regional air quality throughout an entire ozone season, thus allowing an evaluation of model skill and the efficacy of control options for the full spectrum of meteorological conditions that are encountered over an ozone season.

<u>Modularity:</u> MAQSIP is fully modularized and is thus capable of simulating all relevant physical and chemical processes using various combinations of algorithms available within the system library.

[#] The domain may be subdivided into multiple nested grids

[*] For ~100,000 grid cells (60x57x30) and RADM2 chemistry (58 species)

[†] On Cray T90

Coupling to Environmental Decision Support System (EDSS): The air quality modeling system is integrated into the NCSC—EDSS (Ambrosiano et al, 1995). EDSS provides a computing infrastructure that allows a user sitting at a computer terminal to easily and accurately set-up and execute complicated air quality modeling runs involving multiple and variable modules, couple the air quality model to other relevant and complex decision-making tools (e.g.., econometric models, exposure models, risk analysis), and then visualize and analyze the results.

11.1.2 Specific Features and Options

Emissions

Emitted Species — 15-22 depending upon chemical mechanism.

Point Sources — Fractionated into appropriate vertical grids, distributed uniformly in horizontal grid. *Future plans include addition of plume-in-grid system.*

Area Sources — Uniform over surface grid cell.

Grids/Spatial & Temporal Resolution

Grid — Generalized coordinate system. UTM or Lambert-conformal map projections in horizontal. Sigma-p in vertical for hydrostatic simulations. Sigma-z in vertical for non-hydrostatic simulations.

Horizontal Res. — Highly flexible: 18-80 km for regional scales, 2-6 km for urban scales. Multiple, multi-level deep nests using one- and two-way nesting.

Vertical Res. — Non-uniform grid spacing in the vertical (up to 30 layers have been used in current applications)

Temporal Res. — Time steps determined by characteristic times of transport and chemistry processes. Chemical fields saved hourly. Four month continuous simulation capability covering entire ozone season.

Chemistry

Gas-Phase Chemistry — Updated CB-IV and RADM2 with vectorized numerics/solution. *Future plans call for addition of SAPRC*

Photolysis Rates	Madronich scheme. **Future** *plans call for addition of explicit radiative transfer calculations interactive with clouds and aerosols.*
Aqueous-Phase Ch.	Modified Walcek mechanism using resolved-scale and convective cloud fields from meteorological model.
Aerosol Chemistry	Nighttime oxidation of N_2O_5, and explicit treatment of aerosol dynamics using Regional Particulate Model (RPM) sulfate/ammonia mechanism. *Future plans call for addition of organic and nitrate aerosols.*

Meteorology, Transport, Dispersion

Meteorology	Prognostic model. Current applications use MM4, Non-Hydrostatic MM5, RAMS.
Transport	3-D winds. Vertical wind derived from continuity equation for hyrdostatic simulations.
Vertical Diffusion	Derived from met fields using K-theory *Future plans call for additional options including TKE, Transilient, ACM schemes for turbulent closure*
Cloud Pumping	Shallow convection using Betts-Miller parameterization and deep convection using Kain-Fritsch parameterization.
Numerical Solution/	Smolarkiewicz, Yamartino, Dabdub and Seinfeld (ASD), and Bott schemes,
Transport Scheme	Piecewise Parabolic Method, Flux Corrected Transport, Semi-Lagrangian Transport, and Chapeau Function Method.

Clouds/Deposition

Radiation	Attenuation of solar radiation by clouds.
Wet Deposition	In-cloud and below-cloud scavenging
Dry Deposition	Resistance in series for gases. Size-dependent resistant model for aerosols.
Transport	Deep and shallow convection (see above).

Section 12: Appendix B

12.1 Breakdown Of MAQSIP Modules and Routines

12.1.1 Module driver_ngc

driver.F
proces.F

12.1.2 Module convert_ngc

convert.F
inbdycon.F

12.1.3 Module init_ngc

initscen.F

12.1.4 Module getstep_ngc

getstep.F

12.1.5 Module bot_ngc

hadvbot.F
zadvbot.F
advbot_h.F
advbot_z.F
adj_con.F

12.1.6 Module eddy_ngc

hdiff.F
vdiff.F
edyintb.F
tridiag.F

12.1.7 Modules radm2_mqssa_ngc and cb4_ngc

chemsolv.F
gaschem.F
phot.F
pq1.F

rateconst.F

rated.F

12.1.8 Module radm_cloud_ngc

cldproc.F

cldprocr.F

12.1.9 Modules sigma_p_hyd and sigma_p_nhy

calcmet.F

height.F

hcontvel.F

vcontvel.F

hcontdiff.F

vcontdiff.F

depcontvel.F

12.2 LIST OF REQUIRED EXTERNAL INCLUDE FILES

12.2.1 IOAPI Declarations

PARMS.EXT

FDESC3.EXT

IODECL3.EXT

12.2.2 I/O File Declarations

FILES3.EXT

12.2.3 Needed Constants

CONST3.EXT

12.2.4 Memory Size Declarations

HGRD.EXT

VGRD.EXT

SPCS3_XXXX.EXT

12.2.5 Species Lists For Transport Processes

ADV3_XXXX.EXT

DIF3_XXXX.EXT

DDEP3_XXXX.EXT

EMIS3_XXXX.EXT

12.2.6 Chemistry Processor Declarations

CHEMCONST.EXT
MECHANISM.EXT
PHOTLYTK.EXT

12.2.7 Cloud Processor Declarations

CLDAQ3_XXXX.EXT
WDEP3_XXXX.EXT

SECTION 13: APPENDIX C

13.1 REQUIRED DATA FILES

GRID_BDY_2D

MSFX2		squared map-scale factor (CROSS)	
PSTAR0	*Pa*	pressure difference	NHYD

GRID_CRO_2D

LAT	deg	latitude (south negative)	
LON	deg	longitude (west negative)	
MSFX2		squared map-scale factor (CROSS)	
HT	*m*	terrain elevation	
PSTAR0	*Pa*	pressure difference	NHYD

GRID_DOT_2D

MSFD2		squared map-scale factor (DOT)

GRID_BDY_3D

DENS0	$\frac{kg}{m^3}$	reference density	NHYD

GRID_CRO_3D

ZH	*m*	mid-layer height above ground	NHYD
ZF	*m*	full-layer height above ground	NHYD
DENS0	$\frac{kg}{m^3}$	reference density	NHYD

MET_BDY_2D

PSTAR	*Pa*	pressure difference	HYD

MET_CRO_2D

VDEP	$\frac{m}{s}$	deposition velocity for deposited species	
PBL	m	planetary boundary layer height	
USTAR	$\frac{m}{s}$	horizontal friction velocity	
WSTAR	$\frac{m}{s}$	convective velocity scale	
MOL	$\frac{1}{m}$	inverse Monin-Obukhov Length	
RN	cm	accumulated nonconvective precipitation	
RC	cm	accumulated convective precipitation	
WBAR	$\frac{g}{m^3}$	average liquid water content of clouds	
CLDB	m	cloud bottom	
CLDT	m	cloud top	
CFRAC		total fractional cloud coverage	
PSTAR	Pa	pressure difference	HYD

MET_BDY_3D

DENS	$\frac{kg}{m^3}$	air density

MET_CRO_3D

TA	K	air temperature	
QV	$\frac{g\ water}{g\ air}$	specific humidity	
PRES	Pa	air pressure	
DENS	$\frac{kg}{m^3}$	air density	
WWIND	$\frac{m}{s}$	vertical component of wind	NHYD
ZH	m	mid-layer height above ground	HYD
ZF	m	full-layer height above ground	HYD

MET_DOT_3D

UWIND	$\frac{m}{s}$	u component of horizontal wind
VWIND	$\frac{m}{s}$	v component of horizontal wind

CHEM_BDY_3D

BCON   *ppm*   boundary concentrations

CHEM_INIT_3D

ICON   *ppm*   initial concentrations

CHEM_EMIS_3D

EMIS $\frac{g}{s}$ emitted concentrations